Ionic liquids for enhancing alkaline water electrolysis

Szilveszter Gábor Kéki

Thesis to obtain the Master Science Degree in

Energy Engineering and Management

Supervisors: Dr. Diogo Miguel Franco dos Santos

Dr. Biljana Šljukić Paunkovic

Examination Committee

Chairperson: Prof. Francisco Manuel da Silva Lemos

Supervisor: Dr. Diogo Miguel Franco dos Santos

Member of the Committee: Prof. Ivana Stojković Simatović

October 2020

Acknowledgements

First of all I would like the express my special thanks to my supervisors Dr. Biljana Šljukić Paunković and Dr. Diogo Miguel Franco dos Santos who supported and help me during the experiments and to put my results and words in this thesis. Without them, it would have been even more hard to prepare this study. Then, special thanks to Raisa Oliveira who helped me a lot in the lab. Finally I also would like to say thanks to my parents and to my cousin Bertalan Stark who were supporting me at home in Hungary.

Abstract

Alkaline electrolysis is the most mature technology to produce hydrogen gas from electricity. Using electricity from renewable sources thus, makes an opportunity to prepare green energy carrier as hydrogen gas, which can help the economy to switch from carbon-based fuels to green and sustainable sources. However, nowadays 96% of hydrogen production is based on steam reforming, using fossil fuels. In order to make electrolysis competitive towards steam reforming, enhancing the hydrogen and oxygen evolution reaction (HER and OER) is essential. Besides selecting proper electrocatalytic materials the activation overpotential could be decreased by electrolyte additives, such as room temperature ionic liquids (RTILs). Previously the catalytic effect of RTILs on HER was confirmed in acidic and in alkaline solutions as well. Because RTILs could be easily modified, the catalytic effect on HER and OER of new types of RTILs, namely: a) 3-Ethyl-1-methylimidazolium chloride (C2); b) 3-Butyl-1-methylimidazolium chloride (C4); c) 3-(2-Methoxyethyl)-1-methylimidazolium chloride (C1OC2); and d) 3-(2-Ethoxyethyl)-1-methylimidazolium chloride (C2OC2) were tested in this study. Cyclic voltammetry at 25 ºC; linear scan voltammetry at 25 ºC, 40 ºC, 50 ºC, 60 ºC, 70 ºC and 80 ºC; and chronoamperometry at 25 ºC and 80 ºC with Pt electrode are used to study the addition of small amount (1 V/V%) of the listed RTILs on HER and on OER in alkaline solution. Kinetic parameters are calculated. Afterward with the RTIL that performed the best, volume measurements were done to compare the gas production in pure 8M KOH solution, and the gas production with the addition of the chosen RTIL in a small-scale alkaline electrolyzer.

Key words

Room temperature ionic liquids; alkaline electrolysis; HER; OER; electrolyte additives

Resumo

A eletrólise alcalina é uma tecnologia madura para produzir hidrogénio sem recurso a combustíveis fósseis. O uso de eletricidade proveniente de fontes renováveis permite produzir hidrogénio verde, ajudando a economia a mudar de fontes de energia baseadas no carbono para fontes de energia verdes e sustentáveis. No entanto, 96% da produção de hidrogénio é baseada na reformação com vapor de água, utilizando combustíveis fósseis. Para tornar a eletrólise competitiva em relação à reforma a vapor, é essencial aumentar a eficiência das reações de evolução de hidrogénio e oxigénio (HER e OER). Além disso, usando elétrodos adequados, a sobretensão de ativação pode ser diminuída por meio de aditivos eletrolíticos, como líquidos iónicos à temperatura ambiente (RTILs). Sabe-se que é possível aumentar a cinética da HER na presença de RTILs em soluções ácidas e alcalinas. Como os RTILs podem ser modificados, este estudo examinou o efeito na cinética da HER e OER de novos tipos de RTILs, nomeadamente: cloreto de 3-etil-1-metilimidazólio; cloreto de 3-butil-1-metilimidazólio; cloreto de 3-(2-metoxietil)-1-metilimidazólio; e cloreto de 3-(2-etoxietil)-1-metilimidazólio. Voltametria cíclica, voltametria de varredura linear e cronoamperometria foram realizadas a diferentes temperaturas (entre 25 e 80 ºC) usando elétrodos de Pt para estudar o efeito da adição de uma pequena quantidade (1 vol.%) dos RTILs listados na cinética da HER e da OER em solução alcalina. Determinaram-se vários parâmetros cinéticos. Adicionalmente, mediu-se o volume de gás produzido num eletrolisador alcalino de pequena escala para comparar a produção numa solução de 8 M KOH antes e após adição do RTIL selecionado.

Palavras-chave

Líquidos iónicos à temperatura ambiente; eletrólise alcalina; HER; OER; aditivos eletrolíticos

INDEX

List of Figures

List of Tables

List of Abbreviations

Abbreviations	***Explanation***
AEL	Alkaline electrolysis
C1OC2	Methoxyethyl)-1-methylimidazolium chloride
C2	3-Ethyl-1-methylimidazolium chloride
C2OC2	3-(2-Ethoxyethyl)-1-methylimidazolium chloride
C4	Butyl-1-methylimidazolium chloride
CA	Chronoamperometry
CV	Cyclic voltammetry
ECAS	Electrochemically active surface area
EDL	Electrolytic double layer
FTIR	Fourier transform infrared
GC	Glassy carbon
HER	Hydrogen evolution reaction
IEA	International Energy Agency
IL	Ionic liquid
LSV	Linear scan voltammetry
OCP	Open circuit potential
OER	Oxygen evolution reaction
ORR	Oxygen reduction reaction
P2G	Power to gas
PE	Plasma electrolysis
PEC	Photoelectrochemical cell
PEM	Polymer electrolyte membrane electrolysis
PEMEL	Proton exchange membrane electrolysis
RDS	Rate-determining step
RE	Renewable energy
RTIL	Room temperature ionic liquid
SDS	Sustainable development scenario
SOE	Solid oxide electrolysis
STP	Standard conditions for temperature and pressure
TiPES	Tipping points in the earth system

Chapter 1: Introduction

This study aims at investigating the catalytic potential of adding room temperature ionic liquids (RTILs) to enhance the efficiency of water electrolysis in alkaline solution. The work focuses simultaneously on the hydrogen evolution reaction (HER) and the oxygen evolution reaction (OER), since OER kinetics are the core barrier of the reaction and makes water electrolysis less efficient [1, 2]**.**

1.1. Global overlook

In the 21st century, the greatest challenge of humanity is to minimize the impact of global warming. The Paris Agreement's long-term temperature goal is to "keep the increase in global average temperature to well below 2 ºC above pre-industrial levels; and to pursue efforts to limit the increase to 1.5 ºC, recognizing that this would significantly reduce the risks and impacts of climate change" [3]. For instance, below 2 ºC of increase, there is a smaller probability that the Greenland ice sheet will shrink in a way that will induce irreversible changes in the climate system. The Greenland ice sheet is a tipping element – a substantial part of the global climate system - and a critical amount of shrinking of the ice sheet could be considered as a tipping point, which if it takes place, the climate system could shift permanently. The Earth has several tipping elements (see **Table 1**), and each has a tipping point such as the loss of the Arctic ice sheet, which can shut down the Atlantic thermohaline circulation (see **Figure**

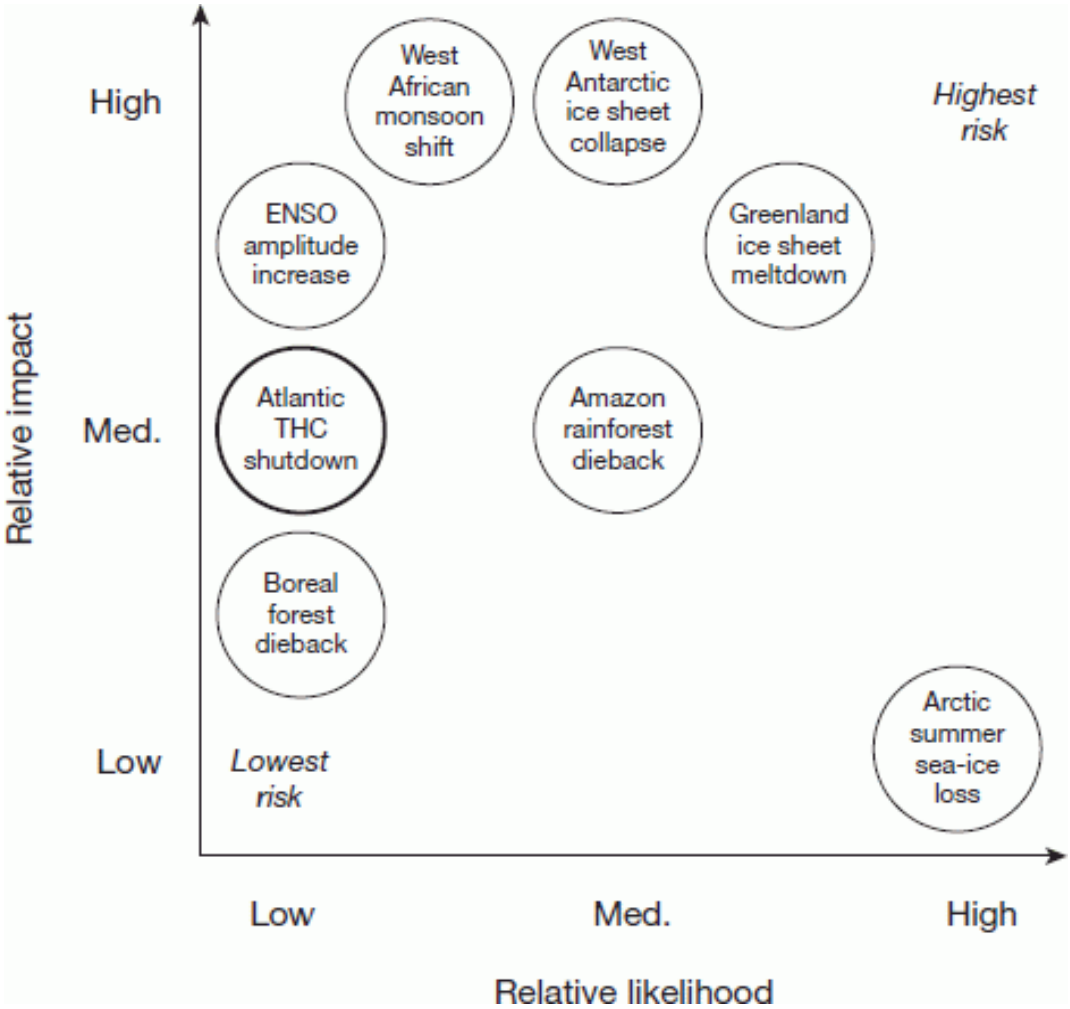

Figure 1. *A 'straw-man' risk matrix for climate tipping points [45].*

1) [4]. Therefore, if any of these phenomena occur, they are increasing the possibility of others to happen, and these synergies can make an abrupt domino effect. That is why it is important to keep the global temperature rising below 2 ºC to ensure that the climate system is not going to change in a dramatic way.

However, besides the growing agreement among scientists that many subsystems of Earth's climate will behave nonlinearly at a certain level – previously described as tipping points - forced by anthropogenic activity, state-of-the-art Earth System Models cannot imitate those abrupt shifts in the climate system that occurred in the past. To overcome this problem a new project called TiPES just launched this September 2020, in order to understand much more clearly how our climate system is working, and to identify exact values of tipping points that we must not over exceed in the future [5].

Table 1. *Brief summary of risks related to different regions or phenomena of Earth's climate system under different global average temperature increases (above preindustrial level)* [6].

Phenomenon	Warming of 1.5 ºC or less	Warming of 1.5 ºC–2 ºC	Warming of 3 ºC or more
Permafrost	30.5% reduction in permafrost (4.8 Mkm^2) (medium confidence) Irreversible loss of stored carbon	42.5% reduction in permafrost (6.6 Mkm^2) (medium confidence) Irreversible loss of stored carbon	Potential for permafrost collapse (low confidence)
Rainforests	Reduced biomass, deforestation and fire increases pose uncertain risks to forest dieback	Larger biomass reductions: deforestation and fire increases pose uncertain risk to forest dieback	Rainforests in Central America reduced by 40% Potential tipping point leading to marked forest dieback (medium confidence)
Heat waves	13.8% of the world population would be exposed to 'severe heatwaves' at least once every 5 years	36.9% of the world population would be exposed to 'severe heatwaves' at least once every 5 years	Substantial increase in potentially deadly heatwaves very likely
Coral reefs	Loss of 70–90% of coral reefs	Loss of most coral reefs (99%) and weaker remaining structures owing to ocean acidification	Loss of most coral reefs (very likely)
Agricultural systems: crop yield	Reduction in global maize crop production ~10% 35 Mppl exposed to lower crop yield	Reductions in global maize production ~15% 362 Mppl exposed to lower crop yield	Collapse of maize crop in some regions (low confidence) 1817 Mppl exposed to lower crop yield
NPV of climate change induced damages	54 trillion USD	69 trillion USD	551 trillion USD

**(including market, non-market impacts, impacts due to sea level rise and impacts associated with large scale discontinuities)*

1.1.1. How to stay below the 2 ºC increase? Future scenarios related to energy consumption

The International Energy Agency (IEA) provides a sustainable development scenario (SDS) to forecast future energy consumption in 2040. The SDS is fully in-line with the long term objectives of the Paris Agreement and is aiming to maintain the global energy consumption on the current level (2017, 13972

Mtoe), meanwhile cutting drastically CO_2 emissions (32.5 →17.5 Gt energy related CO_2 emission) by increasing the share of renewable energy (RE) sources in the final energy consumption [7].

Currently 50% of the final energy consumption is related to heat (industry 46%, buildings 49%) and ~28% related to the transport sector which can be interpreted to global CO_2 emissions share, thus, heat production is responsible for the 33% and transport sector for the 22% of global CO_2 emission. However, the share of REs in the transport sector is only 3.5%, and in the heating sector it is only 10% [7, 8]. According to the SDS we have to rise RE share in the heating sector up to 25% and in transport up to 19%, meanwhile the RE shares in electricity production should rise up to 66% from 25% until 2040 [7]. However according to IEA's data, in 2017 in the share of Solar PV and Wind energy in electricity generation are only 1.7% for PV and 4.2% for Wind [7] and these RE sources are already making grid-stability problems due to their high temporally fluctuations [9, 10]. It is obvious that with the prediction of SDS these stability issues become more impactful since the share of Wind energy should rise to 21.7% and the share of Solar PV is expected to rise as well up to 18% in electricity generation.

Power to gas (P2G) technology provides us to store electric energy in the form of hydrogen or methane. Methane is produced from hydrogen and CO_2 by methanation process. Both H_2 and methane can be used as fuel for transportation (in combustion engines and fuel cells) and for heating purposes. So far, the pipeline system for natural gas is already installed worldwide, hence in the close future P2G could offer a large-scale long-term storage option for electricity, which can solve grid stability issues related to Solar PV and Wind energy.

Water electrolysis is used for transforming electricity into hydrogen. Today primarily alkaline and polymer electrolyte membrane (PEM) electrolysis is used in commercial applications. These are called low temperature electrolysis because they are operating below 100 ºC. There is a third promising way of high temperature electrolysis called solid oxide electrolysis, which could improve efficiency, but it is still in R&D state and needs improvements.

From all of them, alkaline electrolysis is the most used technology, thanks for the comparably lower cost, and better endurance. Therefore, this study is aiming to improve alkaline electrolysis because it is the most embedded technology in general [8].

1.2. Hydrogen production

Nowadays hydrogen plays an important role, especially for industrial purposes, like feedstock for fertilizers, petroleum refining processes, petrochemical industry, or fuel cells, for the chemical industry and for methanol, ammonia, and steel production processes [11, 12]. Around 500 billion Nm^3 of hydrogen is produced every year. Since steam reforming is the cheapest way to produce it, 96% of hydrogen is produced in this way. This method uses fossil fuels as a carbon source, namely 48% for steam reforming of natural gas, 30% for oil and naphtha reforming, 18% for coal gasification, and only 4% for electrolysis. These carbon sources not just emit a large amount of CO_2, but also release harmful gases such as SO_x, NO_x, and CO [13].

Although hydrogen has a great potential to contribute to a stable and green energy access, currently the fossil-based hydrogen production emits 830 million tons of CO_2 each year, which is around 2.4% of the global CO_2 emission (global emission: 35 000 Mt CO_2/year). In terms of CO_2 emission intensity, 10

kg of CO_2 is released after each produced kg of hydrogen from natural gas, 19 kg CO_2 per kg of hydrogen from coal and 12 kg CO_2 per kg of hydrogen from oil [14, 15]. Therefore, alternative CO_2 free hydrogen production ways are mandatory in order to use hydrogen as an energy carrier.

Electrolysis is the only commercialized technology that will be able to compete with fossil-based hydrogen production ways. But before showing electrolysis current state, let us look at the other alternative hydrogen production methods:

- Thermolysis is based on the concept that water can break straight to hydrogen and oxygen at high temperature. Without any chemical additives, it is occurred at around 2000 ºC which still makes it impossible to use such materials in order to make the process economically feasible. To overcome the problem with the high temperature, it is possible to combine thermolysis with special chemical reactions like- two-step cerium oxide thermal cycle, - "hybrid" copper chloride cycle or sulfur-iodine cycle, and as a result the water decomposition temperature is decreased to 900 ºC. The technology called thermochemical water splitting, it could the sun or nuclear power as a heat source, but the commercialization of the technology is expected in long term [12, 16].
- There are also biological ways to produce CO_2 free hydrogen. Anaerobic bacteria can convert biomass into hydrogen, during the dark fermentation process or algae can do the same in the presence of light through photo fermentative process. However, the high reactor volume needs, the low efficiency and the low yield are still the main disadvantages [12].
- Photoelectrochemical cell (PEC) is another field of interest. It uses the same semi-conductor materials as photovoltaic panels, but the generated electrons are directly used to split water instead of creating a current. However, PEC systems are very young, and so far, they are combined with PV technology to absorb a wider range of the solar spectrum. Although 10% of solar to hydrogen efficiency is already achieved by a PEC/PV system, called PEC/perovskite solar cells, it requires further improvements in terms of materials, cell design process stability etc. [17].
- Biomass gasification has already proved its own commercial feasibility in several plants [18]. During biomass gasification the same thermochemical reactions represent an in fossil fuel based technologies, namely – pyrolysis, -partial oxidation, -steam reforming, but the carbon source in this case is biomass [12]. The drawbacks of biomass gasification are the lower efficiency comparing to fossil-based gasification and the formation of tars [19]. Although biomass gasification can offer similar economic feasibility as alkaline electrolysis, it requires 2-3 times higher investment cost [18], and moreover to satisfy the same hydrogen demand, biomass gasification requires 17 times more land area, comparing to wind power based alkaline electrolysis [15].

To compete with fossil-based hydrogen production, production cost has to be reduced to a comparable level. This price is around 1 \$/kgH_2 from coal, and 1.8 €/kgH_2 from natural gas in China. In the future it is expected that carbon capture technology will be forced to the producers, which is increasing the fossil based priced by 20% [15]. Nowadays water electrolysis is treated as the only competitive technology in

terms of large-scale CO_2 emission less hydrogen production against the fossil-based thanks. The main reasons are the followings:

- Alkaline systems are already scaled up to 2 MW single stack capacity, which has a CAPEX of 750 €/kW, and is projected to decrease below 500 €/kW in case of 100 MW power input.
- This value is considered to be decreasing due to further scaling up.
- By state-of-art data, 3 €/kg H_2 production cost is rational by 2020
- If electricity price decreases by the emerging of solar PV and wind power farms the cost goes further below 3 €/kg H_2. The expected hydrogen production price is shown in **Figure 2.** as a function of full load hours, considering 450 USD/kW CAPEX, 30 years as the lifetime of the electrolyzer system, efficiency is 70%, the steam methane reforming cost arrange from 1-3 USD/kg [20].

As we can see, the number of required full load hours are not enough yet to provide a competitive production price for electrolyzers. However, as mentioned before, according to the Sustainable Development Scenario (SDS), there will be a big jump in the Wind and Solar PV power generation, from 435 TWh to 6409 TWh in the case of PV solar, and from 1085 TWh to 7730 TWh in case of Wind. This indicates that the full load hours of electrolyzer will rise at the same time that there will be cheaper electricity. Electrolysis systems are increasing the storage capacity of the electric grid. Meanwhile the higher capacity helps the further penetration of renewables (mainly PV and Wind power), which should indicate a drop in electricity price, making electrolyzers more feasible (see **Figure 2**). This synergy between renewables and water electrolysis technologies has great potential for carbon free hydrogen production.

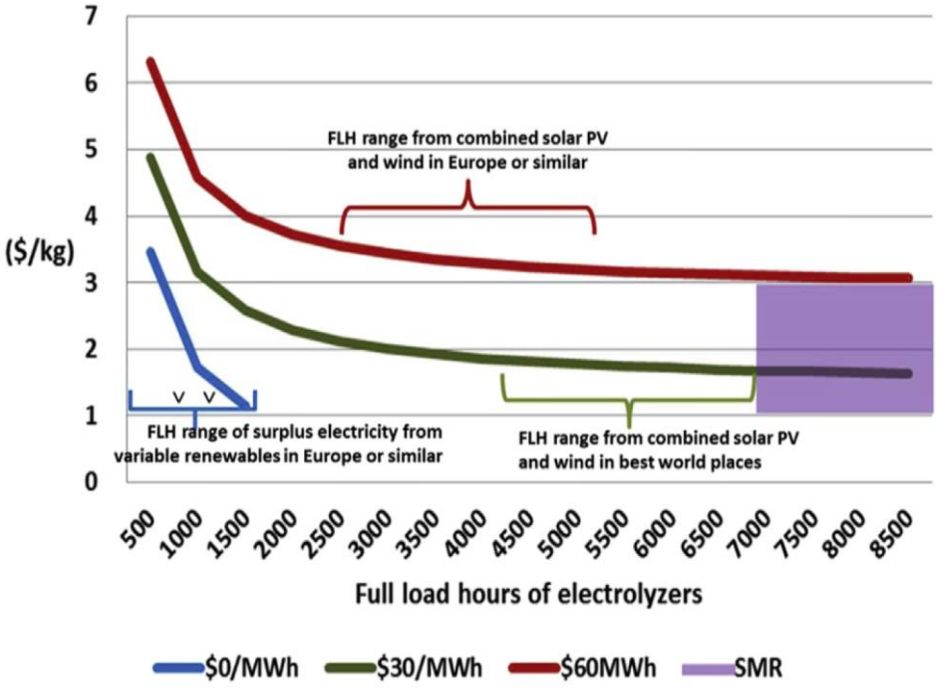

Figure 2. *Hydrogen production cost [USD/kgH2] by electrolysis as the function of full load hours [20].*

1.3. Electrolysis

During water electrolysis an external DC power source is applied, which splits water into hydrogen and oxygen. The basics of the idea was demonstrated in the 19th century by J.W. Ritter. At the end of the century around 400 electrolyzers were already used in the industry [13]. There are three water electrolysis technologies being commercialized, namely alkaline electrolysis (AEL) proton exchange membrane electrolysis (PEMEL) and solid oxide electrolysis (SOE) (see **Figure 3**).

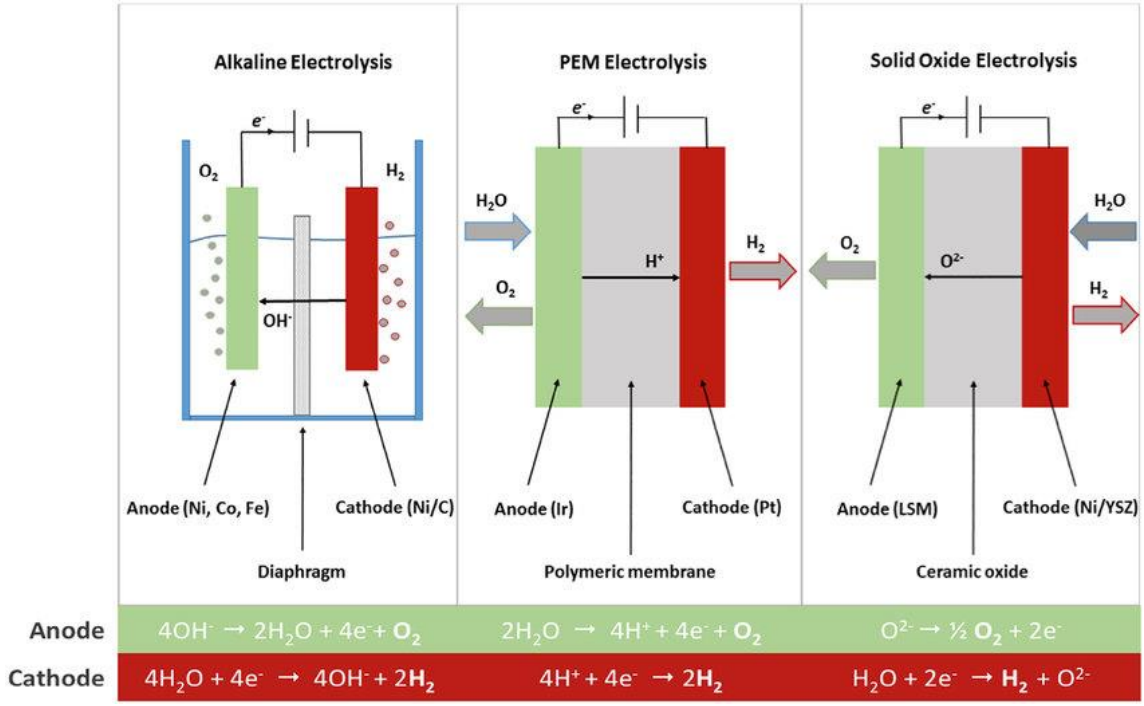

Figure 3. *Schematic diagram of AEL, PEMEL and SOE, including the general anode and cathode reactions I [23].*

Because alkaline electrolysis was developed first, this is the most mature and commercialized from all of them, therefore it is scaled up the most, respectively 2 MW for a single stack system. The cell is composed by a cathode and an anode, which are separated by a diaphragm. The electrolyte is a KOH or NaOH solution, with the concentration ranging between 20-40 wt.%. The disadvantages of the technology are: - slower start up time from cold to minimum load 20 min-hours,- higher cell area ~4 m^2, -higher minimum load 20%, - slower ramp-up speed 0.13-10%/sec, - lower hydrogen purity 99.5%, - lower operating pressure 1-30 bar and smaller current density 0.2-0.4 A cm^{-2}. However, its longer lifetime – 60 000 - 90 000 h – and the lower CAPEX makes it economically more favorable than the other two water electrolysis technologies [21].

The first PEMEL was developed by the General Electric Co. to correct the imperfections of AEL. In PEMEL the electrodes are separated by a highly acidic proton exchange membrane. The membrane is also fulfilling the role of the electrolyte, thus is also called a solid electrolyte. It also means that on the cathode, there is only the gaseous phase of hydrogen, without any liquids. Summing up the process is similar to the reversed process of the PEM fuel cell technology. Thanks to its design, PEMEL cell produce much higher purity hydrogen (99.9999 vol.%), the operating pressure is higher (30-80 bar), the

current density is also higher (800-2500 mA cm^{-2}) [22], it has a faster start up time from cold to minimum load 5-20 min and it also has more rapid system response [21]. On the other hand, PEMEL electrodes need more expensive catalysts such as Pt/Pd for hydrogen evolution reaction (HER) and IrO_2/RuO_2 for oxygen evolution reactions (OER). In addition, the highly corrosive membrane requires expensive resistant components, and currently PEMEL systems have lower lifetime compared to AEL (~50 000h) [12, 17].

Solid oxide electrolysis (SOE) can allow higher energy efficiency. The process operates between 500 and 850 ºC, and splits water from steam [12]. The advantage of SOE is that at such a high temperature it is offering the highest electrical efficiency compared to others (81% for SOE, 70% for AEL and 60% for PEMEL [15]). It is also favourable that SOE uses non noble metal catalysts and can offer high-pressure operation (like PEMEL). On the other hand, the ceramic oxide layer, which separates the anode and the cathode, has weak durability due to the high heat stress and, therefore, this technology still requires further developments [23].

1.4. Fundamentals of HER and OER

The overall cell reaction during water electrolysis can be expressed as the following equation (**eq. (1)**) [24]:

$$H_2O \rightleftarrows H_2 + \frac{1}{2}O_2 \quad (1)$$

The anode reaction (**eq. (2)**) [24] in alkaline cell corresponds to:

$$4\,OH^- \rightleftharpoons 2\,H_2O + O_2 + 4\,e^- \quad (2)$$

The cathode reaction (**eq. (3)**) [24] in alkaline cell corresponds to:

$$2\,H_2O + 2\,e^- \rightleftharpoons 2\,OH^- + H_2 \quad (3)$$

The minimum energy, which is required to the reaction can be expressed from the Gibbs free energy (**eq. (4)**) [12]:

$$\Delta G = nFE_0 \quad (4)$$

where: n = number of electrons involved

F = 96500 (Faraday constant)

E_0 = reversible potential

ΔG for water splitting at STP conditions is 237.22 kJ/mol, which let us calculate the reversible cell voltage (**eq. (5)**):

$$E_{rev} = \frac{\Delta G}{nF} = \frac{237220}{2 \cdot 96500} = 1.23\,V \quad (5)$$

On the other hand, we have to consider that during water spitting entropy is generated, therefore using enthalpy (ΔH) (**eq. (6)**) instead of Gibb's free energy (ΔG) is more adequate [12]:

$$\Delta H = \Delta G + T \cdot \Delta S = 237.22 + 298.15 \cdot 0.16318 = 285.87\,kJ\,mol^{-1} \quad (6)$$

where T = 298.15 K as room temperature

ΔS = 0.16318 kJ mol^{-1} K^{-1} as the entropy of the reaction

The minimum cell voltage, related to the enthalpy of the reaction, is also called the thermoneutral cell voltage (E_{TN}) [13], and can be expressed by **eq. (7)** :

$$E_{TN} = \frac{\Delta H}{nF} = \frac{285870}{2 \cdot 96500} = 1.48\ V \tag{7}$$

To calculate the real electric cell voltage, we have to take into account the overpotentials on the anode (η_a) and as well on the cathode (η_c), and we have to consider the ohmic drop ($j \cdot R_{total}$) (**eq. (8)**)in the system which is caused by the sum of: -membrane resistance(R_{memb}); resistance of the circuit (R_{circ}); - resistance of the electrolyte (R_{elec}); bubble resistance (R_b) [13]:

$$i \cdot R_{total} = i \cdot (R_{memb} + R_{circ} + R_{elec} + R_b) \tag{8}$$

The overall cell voltage can be expressed as **eq. (9)** [13]:

$$E = E_{rev} + |\eta_a| + |\eta_c| + i \cdot R_{total} \tag{9}$$

Where: E_{rev}= reversible cell voltage, it is worth mentioning that other authors use the thermoneutral cell voltage [24].

η_a = the anodic overpotential

η_c = the cathodic overpotential

i = the circulating current

R_{total}= the overall resistance

Advanced cell design and new membrane technology can reduce the ohmic drop, while electrocatalysts are aiming to reduce overpotentials. Three main electrocatalytic kinetic parameters are used to evaluate the performance of an electrocatalyst: overpotential (η); Tafel slope (b) and exchange current density j_0. Using the Nernst equation, the applied potential can be written as the followings (**eq. (10)**) [24]:

$$E = E^O_{rev} + \frac{RT}{nF} \cdot \ln\left(\frac{C_O}{C_R}\right) \tag{10}$$

where: E^O_{rev}= reversible potential of the reaction

T= absolute temperature

F= Faraday constant

n = number of electrons involved in the reaction

C_O= concentration of oxidized species

C_R= concentration of reduced species

R = the universal gas constant

The overpotential (**eq. (11)**) is the difference between the applied potential and the potential referred to equilibrium conditions (E_{eq}) [24]:

$$\eta = E - E_{eq} \tag{11}$$

For water electrolysis it is important to compare overpotentials on the same current density, therefore it is necessary to always state at which current density overpotential was measured, as lower overpotential for the same current indicates better electrocatalytic ability [1].

Tafel slope is derived from the Tafel equation. Namely, Butler-Volmer equation gives the correlation between the current density and the exchange current density as the following **eq. (12)** [24]:

$$j \approx j_0 \cdot \exp\left(\frac{\alpha \cdot n \cdot F \cdot \eta}{RT}\right) \quad (12)$$

where: j = current density

j_0 = exchange current density

α = charge transfer coefficient

F= Faraday constant

η = overpotential

R = universal gas constant

n = number of electrons involved in the reaction

T = absolute temperature

Once, overpotential is expressed from this equation, in non-logarithmic or logarithmic form, Tafel equation is obtained (**eq. (13)**), expressing the overpotential as a function of log(j) [25]:

$$\eta = a + b \cdot \log(j) \quad (13)$$

where: $b = the\ tafel\ slope$

$a = constant$

The exchange current density, j_0, is the current density, j, when the overpotential $\eta = 0$, consequently in **eq. (14)**:

$$j_0 = 10^{-\frac{a}{b}} \quad (14)$$

The "a" constant can be defined as the intercept of the regressed line on the Tafel plot. The Tafel slope also can be expressed as **eq. (15)** [26]:

$$b = \frac{2.303 \cdot R \cdot T}{\alpha F} \quad (15)$$

In the above-mentioned eq. (15) the only unknown is the transfer coefficient α that can provide information about the reaction mechanism. In theory, the transfer coefficient is equal to 0.5 in case of a reversible single electron transfer, if the reorganization energy (λ) is much higher than the overpotential (**eq. (16)**). In this case substituting α as 0.5 in **eq. (15)** the obtained slope is 120 mV dec^{-1} [1]:

$$\alpha = \beta = \frac{1}{2} + \frac{\eta}{\lambda} \quad (16)$$

where: β = symmetry factor

λ =re-organization energy

Usually an electrochemical reaction consists of several reactions following each other. In this case a reaction step can be an electron transfer step or chemical reaction such us association or dissociation, therefore α is defined differently, see below (**eq. (17)**) [1]:

$$\alpha = \frac{n_B}{\nu} + n_r \cdot \beta \quad (17)$$

where: n_B= the number of electrons that transfer back to the electrode before the rate-determining step

$\nu =$ the number of rate-determining steps that have taken place in the overall reaction

$n_r =$ the number of electrons that participate in the rate-determining step.

n_B can be 1 if the rate determining step is an electron transferring reaction or 0 if the rate determining step is a chemical reaction. Briefly summing up the described theory:

- if the first electron transfer reaction is the rate determining step, **eq. (17)** is give 0.5 as a result for α, which corresponds to 120 mV dec^{-1} according to **eq. (15)** [1]
- if the second electron transfer step, is the rate determining step, the calculated slope is 40 mV dec^{-1} according to **eq. (15)** [27]
- if the third electron transfer step, is the rate determining step, the calculated slope is 30 mV dec^{-1} according to **eq. (15)** [1]
- if the rate determining step is the chemical reaction after one-electron transfer reaction, the calculated slope is 60 mV dec^{-1} according to **eq. (15)** [1]

Therefore, measuring the Tafel slope, can help to give insight on which step is the rate determining step. The smaller the slope, the rate-determining step is closer to the end of the multiple-electron transfer reaction. In general, a small value for Tafel slope indicates good electrocatalytic behaviour [1].

The HER consists of three steps, where during the first step a hydrogen atom is adsorbing on the metal surface, and with the addition of an electron a hydroxide ion is also forming. This step is known as the Volmer step, and it is followed by the Heyrovsky step, where the adsorbed hydrogen atom in the presence of a water molecule and an electron releases a hydrogen molecule and another hydroxide ion. During the third step, two already adsorbed hydrogen atoms are forming a hydrogen molecule. The possible reaction steps are described below (**eq. (18-20)** [24].

Volmer step:

$$H_2O + M + e^- \rightarrow MH_{ads} + OH^- \quad (18)$$

Heyrovsky step:

$$H_2O + MH_{ads} + e^- \rightarrow M + OH^- + H_2 \quad (19)$$

Tafel step:

$$2MH_{ads} \rightarrow +H_2 \quad (20)$$

The steps of OER are still a matter of discussion. So far, the common parts of this idea concern the intermittent surface adsorbed species, such as MO, MOH and MOOH. During the first step, the hydroxide ion is adsorbed on the metal surface with the release of an electron (**eq. (21)**) [27]:

$$M + OH^- \rightarrow MOH + e^- \quad (21)$$

After this, the adsorbed OH reacts with another hydroxide ion, and forms an adsorbed oxygen atom, with a water molecule and an electron being released (**eq. (22)**) [27]:

$$MOH + OH^- \rightarrow MO + H_2O + e^- \quad (22)$$

This first step is similar in the studied theories. The following reaction can directly create oxygen gas by the combination of two adsorbed oxygen atoms (**eq. (23)**) [27]:

$$2MO \rightarrow 2M + O_2 \quad (23)$$

Or the MO can create further intermediate MOOH, with the adsorption of another hydroxide ion (**eq. (24)**) [1]:

$$MO + OH^- \rightarrow MOOH + e^- \quad (24)$$

In the last step, the MOOH reacts with the hydroxide ion, forming water, oxygen and releasing one electron (**eq. (25)**) [1]:

$$MOOH + OH^- \rightarrow M + O_2 + H_2O + e^- \quad (25)$$

The problem with this pathway is that is not clear that the MOOH intermediate and the oxygen formation are involving an electron transfer in a single step as it is shown on eq. (24,25), or the electron releasing is an additional step, after the adsorption of a hydroxide ion (**eq. (26-28)**) [27]:

$$MO + OH^- \rightarrow MOOH^- \quad (26)$$

$$MOOH^- + OH^- \rightarrow MOO^- + H_2O + e^- \quad (27)$$

$$MOO^- \rightarrow M + O_2 + e^- \quad (28)$$

In this case, there is an additional chemical reaction step, which can affect the rate of OER. In the literature, the OER steps are still a matter of discussion, and are sometimes described in contradictory theories.

1.5. Advances in alkaline electrolysis

The applied cell voltage is expressed as the followings (**eq. (29)**) [28]:

$$\upsilon_{app}: N_S \cdot (V_{rev} + \upsilon_{act} + \upsilon_{ohm}) \quad (29)$$

where: υ_{app}: the applied voltage

N_S: the number of cells

V_{rev}: the reversible potential of the reaction

υ_{act}: activation overpotential of the reaction

υ_{ohm}: ohmic overpotential

The reversible potential of the reaction is always constant - in case of water electrolysis it is 1.23 V – therefore to improve the process there is two way, one is reducing the overpotential of the reaction or secondly, reducing the ohmic overpotential. The main components of the ohmic overpotential in descending order due to their amplitude:

1. H_2 bubbles on electrode surface
2. Ionic resistivity of the electrolyte
3. O_2 bubbles on the electrode surface
4. Electrode distance
5. Membrane resistivity

The resistivity of the electrolyte can be decreased by increasing the temperature, which contributes to the reaction kinetics enhancement as well. At 240 ºC and 37 bar, high current density (j_0) was reported – namely 2 Acm^{-2} meanwhile the potential stayed below 1.75 V. Theoretically, increasing the pressure

would rise the efficiency. In short term the pressure would reach 60 bar, and in long term period, 100 bar operating pressure is aimed.

In PEM, zero gap configuration is already developed, and the technology is going to emerge in alkaline electrolysis as well. The zero-gap configuration is reducing the resistance between the electrodes, meanwhile it also can offer enhancement in the product purity, which pushes the performance closer to PEM.

Generally, an asbestos diaphragm is used to separate the anode and the cathode part. It is fulfilling his role as a membrane. New polymer materials based on a fluorinated composite of a polysulfone matrix and ZrO_2, known as Zirfon, or on polyphenylene sulfide (Ryton), were studied to substitute the asbestos [28].

The other option for enhancing water electrolysis is reducing the activation overpotential by selecting special electrode materials. These are called electrocatalytic materials, and besides accelerating the reaction kinetics they also stabilize the electrodes. Some commercially used electrode materials are shown in **Table 2**.

Table 2. *Brief list of commercial anode and cathode materials with their performance described by activation overpotential and current density (adapted from [28]).*

Anode				Cathode			
Composition	KOH electrolyte concentration and temperature	j / mA cm^{-2}	oxygen overpotential / mV	Composition	electrolyte KOH concentration and temperature	j / mA cm^{-2}	hydrogen overpotential / mV
Ni+Spinel type Co_3O_4	1M; 25 ºC	100	235	Ti_2Ni	7M; 70 ºC	100	16
Ni	13.5; 90 ºC	100	300	Ni60%Zn40%	6M; 80 ºC	300	225
MnO_x modified Au	0.5M; 25 ºC	10	300	Ni80%Fe18	6M; 80 ºC	300	270
$Ni_{0.2}Co_{0.8}LaO_3$	13.5 90 ºC	100	270	Ni-Fe-Mo-Zn	6M; 80 ºC	135	83

A new and barely studied way for decreasing the activation overpotential is using electrolyte additives such as room temperature ionic liquids (RTILs), which was previously studied by my supervisors, and which is the main topic of my master thesis.

1.6. Room Temperature Ionic Liquids (RTILs)

Room temperature ionic liquids (RTILs) are special salts that are in a liquid state below 100 ºC. The cations and anions are complex ions that have wide structural diversity, and through an appropriate selection these RTILs can be tuned to enhance different electrochemical reactions. Usually, these ion pairs are characterized by low volatility and flammability, nearly zero vapour pressure, by high thermal

and electrochemical stability and with other adjustable properties. Recently the most attractive cation bases are: - pyrrolidinium, - imidazolium, quaternary ammonium and piperidinium, meanwhile the most attractive anions bases are: - tetrafluoroborate $(PF_4)^-$, - bis(trifluorormethanesulfonyl)imide (NTf_2^-), - bis(fluorosulfonyl)imide (FSI^-). RTILs generally enhance the conductivity of the electrolyte solution; however, the specific interaction - between the ions and the electrode materials – still requires further investigation. Nevertheless, excellent low temperature performances are reported in case of batteries, fuel cells and electrolysis devices [29]. In our study, imidazolium-based cations were tested with chloride anion pair.

Previously catalytic effect of Butyl-methylimidazolium $(Bmim)^+$ on HER was described by R.F. de Souza et al. on different electrode materials (platinum (Pt), nickel (Ni), AISI 304 stainless steel (AISI 304 SS) and low carbon steel (LCS)) and more importantly they reported higher currents related to LCS electrode with the IL than for Pt with the IL. Also, in their study the 10 wt%. of IL was the optimal concentration among 1 and 30 wt% [30]. Afterwards, they observed a similar phenomenon with Molybdenum (Mo) electrodes whereas after the addition of Bmim based IL, the Mo electrode performed better than the Pt electrode. They explained their result, with the better adsorption of $Bmim^+$ on Mo electrode surface, and the enhancing proton-donating effect of $Bmim^+$ [31].

Sinergy among IL and different electrode materials - namely 3-triethylammonium-propanosulfonic acid $[TEA\text{-}PS]BF_4$ as IL and Pt, Ni, Glassy Carbon (GC), and 304 SS as electrode materials -was investigated by Fernanda et al. In their results they found that with Pt electrode, HER has two different rate-determining steps (RDS), according to the applied voltage. At low overpotential, the Tafel step (hydrogen desorption) is the RDS, and on high overpotential the Volmer step (hydrogen adsorption) is the RDS. With the 304 SS they considered Volmer step as RDS at low and at high overpotentials. Meanwhile with Ni and GC electrodes, the IL brings the HER steps in quasi equilibrium and both Volmer and Tafel steps could be the RDS. The IL decreased the activation energy, the rate of reduction are the followings: Ni<Pt<304 SS<GC, but it is important to mention that surface roughness was in the following order among electrode materials: Ni<Pt<304 SS<GC, likewise the more rough the surface the higher the active surface area, and the smaller the activation energy. They evinced the catalytic effect of $[TEA\text{-}PS]BF_4$ over HCl solution on HER, and they assumed that the cations form organised channels, perpendicular to the electrode surface, and promote the transport of protons to the cathodic surface, as well as further activating the electrode surface [32].

So far, the catalytic effect of IL on HER was tested in acidic solutions, however, the most commercial water electrolysis technology is alkaline water electrolysis where 6-9 M KOH solution is used. Therefore L. Amaral et al. investigated the effect of a small amount of IL addition (ethyl-methylimidazolium $(Emim^+)$ with different anion pairs 1-2 vol%) into alkaline solution (8 M KOH), with Pt electrodes. They reported that the addition of IL, enhanced the current, increased the Tafel slope and the exchange current density (j_0), meanwhile they observed reduction in the resistance related to charge transfer and related to mass transfer, respectively 50% and 70%, and also the overall impedance was reduced by the IL addition. Langmuir-type hydrogen adsorption was observed, and overall, the ILs enhanced the HER kinetics [33]. Regarding the types of anions, they caused minor differences in the HER enhancement. In their next study, temperature dependence was investigated in the range of 25 ºC – 80 ºC, with the addition of 1

vol.% IL again. In this case imidazolium (Im^+), $Bmim^+$ and 3-hydroxylpropyl imidazolium (C_3OHmim^+) cations compared with salicylate (Sal^-) anion were tested. The IL addition confirmed previous results, however with the increasing of the temperature the beneficial effect downturned, and above 50 Cº there was no significant catalytic effect of IL addition. At the same time, decomposition of IL was observed, and Bmim performed the best [34].

The oxygen evolution reaction (OER) is much slower than HER and require the majority of the overpotential in electrolysis system or as well in fuel cells during oxygen reduction reaction (ORR). Therefore Gui-Rong Zhang et al. investigated the catalytic effect of methylimidazolium (mim^+) based ILs, on ORR, related to the alkyl chain length ([$C_n$mim] [NTf_2], n=2;4;6;10). They found a correlation between the chain length and the catalytic effect of the cations. The longer the alkyl chain, the IL is more likely to form lipid or micelle like structures (see **Figure 4b**). On one hand, it is beneficial because it is protecting the electrode from Pt dissolution and also suppressing the formation of non-reactive oxygenated species on the electrode surface, on the other hand, a too long alkyl chain decreasing too much the electrochemically active surface area (ECAS) of the electrode, which gives lower activity at the end. They found that the optimal chain length is 4, likewise C_4mim IL performed the best. A lower chain length protects less the electrode and the longer chains - by forming lipid-like structures – are blocking electrode area. Although the ORR occurs on the positively charged cathode, they assumed that IL ions would form a charge separated layer formation, with a changing anion-cation rich layer at the electrode surface, whereas the proposition of the ions depends on the magnitude of the electrode surface (see **Figure 4a**). Also, it is demonstrated that even cations can be adsorbed on positively charged metal surfaces.

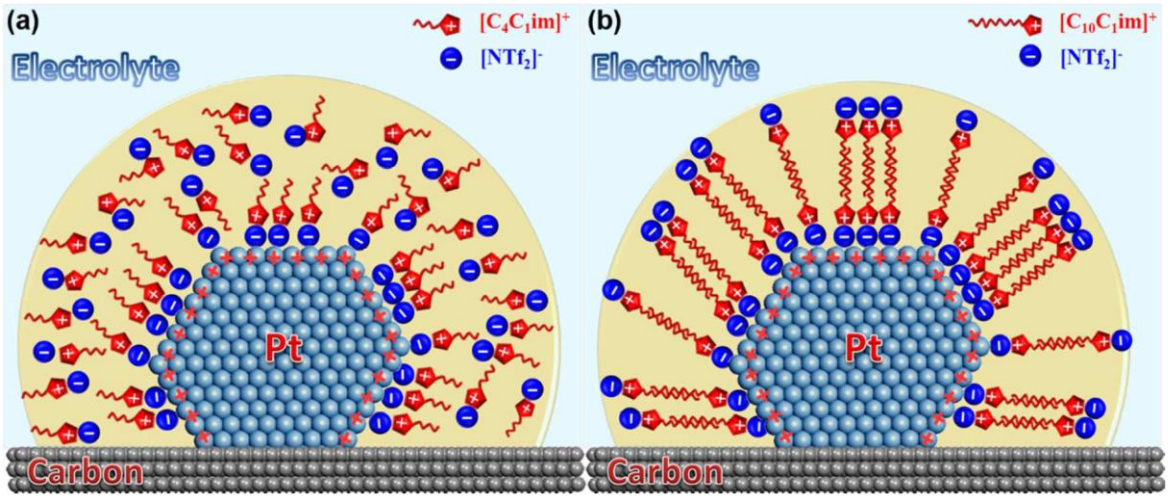

Figure 4. *a) Orientation of IL with short alkyl chain (C2, C4) around positively charged electrode. b)) Orientation of IL with long alkyl chain (C10) around positively charged electrode Source: [35].*

However, it is necessary to highlight that the mechanism of how IL reply to shifting potential and the interactions between ILs and electrode surfaces is poorly described [35].

Leticia Zanchet et al. also investigated the effect of alkyl chain length on imidazolium based ILs. They studied imidazolium (Im^+), methyl imidazolium (MIm^+), and butyl imidazolium (BIm^+) cations, compared with hydrogen sulfate (HSO_4^-) anions. They found that with the elongation of the alkyl chain, the currents, j_0, and the ionic conductivity increasing as well, meanwhile the pH, OCP and the activation energy were decreasing. They reported two Tafel slope region in accordance with previously reported results with Pt electrodes [32], respectively ~30 mV dec^{-1} on low overpotentials, and ~120 mV dec^{-1} on high overpotential region. These results indicated that the ILs make changes in the electrolytic double layer structure, therefore impedance spectroscopy measurements were done as well. They observed decreasing resistance related to H_2 desorption with the elongation of the alkyl chain, in contrast the charge transfer resistance related to H^+ adsorption was increased, but the reduction of overall impedance was higher, as the alkyl chain was longer, confirming previous results of L. Amaral et al. [34]. In their interpretation, the longer nonpolar alkyl chain makes the cation easier to lose its solvation layer, and the less solvated cation can be adsorbed easier on the electrode surface. The adsorbed cation can enhance HER in two ways. Once it is competing with the adsorbed H_2 molecules, thus facilitating H_2 desorption. Secondly, on the N1 position, the nitrogen atom acting as a H^+ donor and acceptor, hence it is participating in the charge transfer process and does not block active sites. These and other results indicate that the IL change the electrolytic double layer (EDL) structure. By measuring the interfacial capacitance between the electrode and the solution at the potential of zero charge, Leticia Zanchet et al. were able to calculate the thickness of the EDL, which is decreasing as the alkyl chain length is growing (see **Figure 5**). [36].

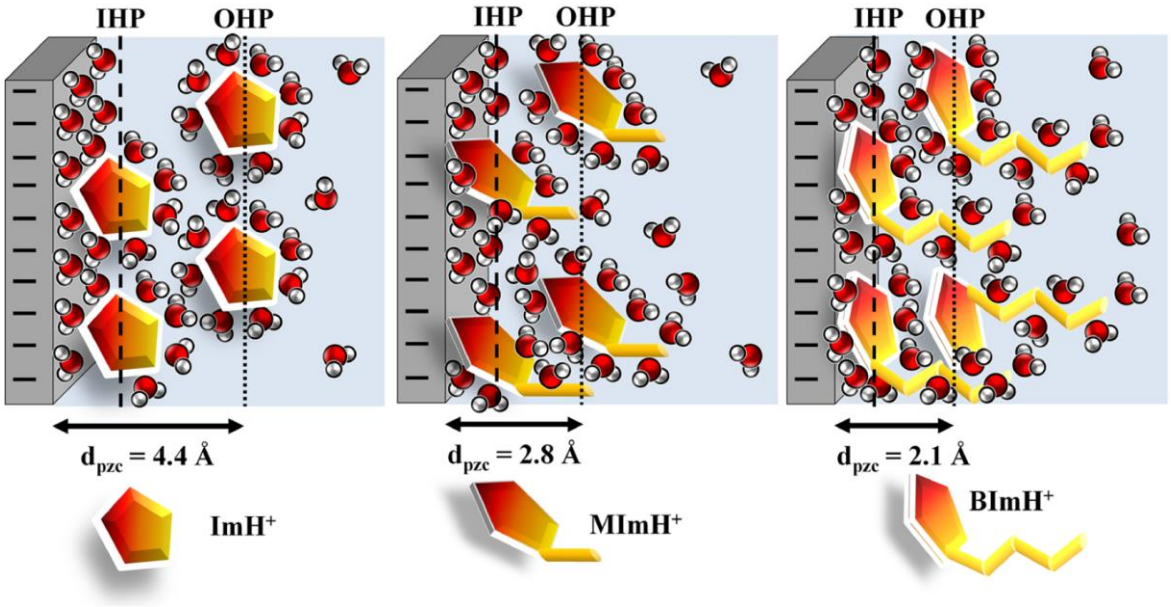

Figure 5. *Illustration of the effect of specifically adsorbed or solvated cations on the EDL, with the corresponding Inner Helmholtz Plane (IHP) and Outer Helmholtz Plane (OHP)Ionics. Source: [36].*

J. Gao et al. studied the degradation of different IL, composed from $[C_nmim]^+$, (n=2;4;6) cations, compared with Cl^-,Br^-, BF_4^- and acetate (Ac^-) anions, using plasma electrolysis (PE) as degradation process. According to their results, the most stable cations are the following in descending order: C_2mim^+> C_6mim^+> C_4mim^+, meanwhile the most stable anions were: Ac^-≈ BF_4^->Br^->Cl^-. During the PE process IL were completely oxidised to NO_2^-, NO_3^- and CO_2. Among the intermediates, there is the oxygenated imidazolium ring, which was detected by other research as well, but after the break of the imidazole ring other intermediate compounds were detected, which were differed from previous degradation tests, due to the different degradation process [37].

Chapter 2: Measurements

The goal of this study is to observe the effect of adding different ionic liquids (ILs) to the electrolyte on hydrogen evolution reaction (HER) and as well on oxygen evolution reaction (OER) during alkaline water electrolysis. All of these four IL have chloride (Cl^-) anion, while the cations are different methyl-imidazolium-based cations. Namely, the four ILs are: a) 3-Ethyl-1-methylimidazolium chloride (C2) (see **Figure 6A**).; b) 3-Butyl-1-methylimidazolium chloride (C4) (see **Figure 6B**); c) 3-(2-Methoxyethyl)-1-methylimidazolium chloride (C1OC2) (see **Figure 6C**); and d) 3-(2-Ethoxyethyl)-1-methylimidazolium chloride (C2OC2) (see **Figure 6D**). Tafel analysis was performed to study ILs addition effect on OER and HER efficiency. With the most promising IL, volume measurement was done to compare quantitatively how much more hydrogen gas can be produced with the same energy investment.

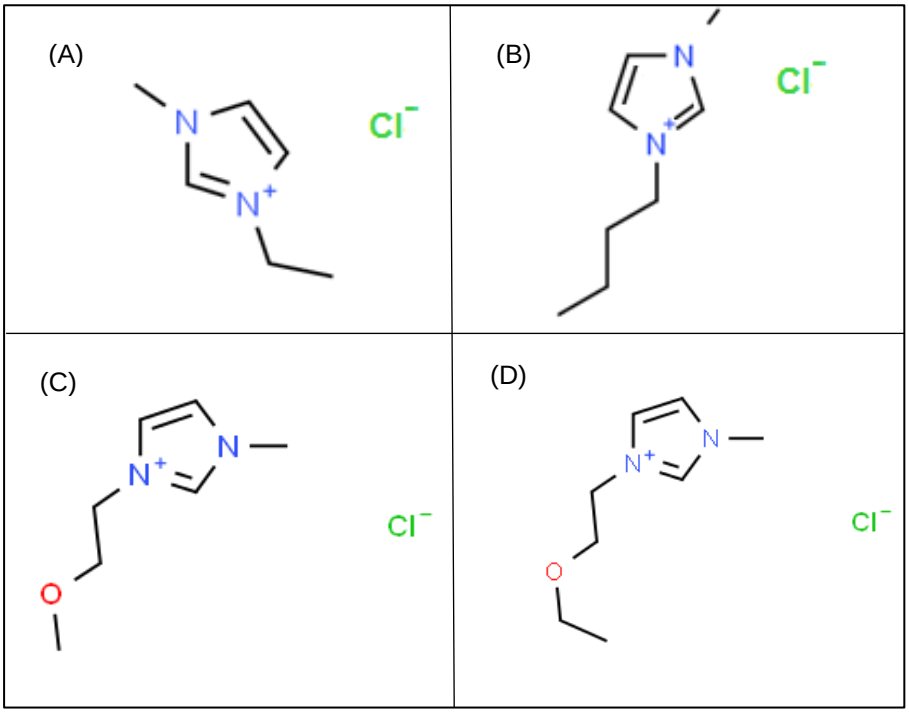

Figure 6. *Chemical structure of the studied ILs sharing the same anion: (A) 3-ethyl-1-methylimidazolium chloride (C2), (B) 3-buthyl-1-methylimidazolium chloride (C4), (C) 3-(2-methoxyethyl)-1-methylimidazolium chloride (C1OC2), (D) 3-(2-ethoxyethyl)-1-methylimidazolium chloride (C2OC2). Source: [45]*

2.1. Equipment

Polarisation measurements were performed with the following equipment:

- Potentiostat: EG&G Princeton Applied Research Potentiostat/Galvanostat 273A
- Software: Power Suite
- Cell volume: 50 ml
- Working electrode: a Pt foil (Metrohm 6.0305.100); surface area 1 cm^2
- Counter electrode: Pt mash; surface area 50 cm^2
- Reference electrode: HANNA instruments HI5412, 3.5M KCl
- Labnet BioPette plus for measuring the added volume of IL

- Metter AE200 for measuring the mass of the added IL
- J.P Selecta, s.a. Termotronic for setting and maintaining different temperatures

For generated gas volume measurements equipment used was:

- Potentiostat: EG&G Princeton Applied Research Squid Potentiostat
- Ritter: MILLIGASCOUNTER Type MGC-1 PMMA
- Software: Rigamo v3.1 by Ritter
- Electrodes: Ni electrodes; surface area 22.4 cm^2

2.2. Ionic liquids

Imidazolium$^+$-based ionic liquids were developed in the 1990's and gained attention thanks to their easy preparation and storage. Herein, four different types of ionic liquids were tested. All of them had Cl^- as anion, and imidazolium$^+$-based cation. The difference among them is the different alkyl groups on the 1-methyl-imidazolium$^+$ ring. In this study, the different alkyl groups were the following:

- 2-methoxyethyl
- 2-ethoxyethyl
- Ethyl
- Butyl

2.3. Electrochemical Measurements

The 8M KOH (AppliChem Panreac 85%) solutions were prepared with Millipore water. After that, 1 vol % of one of four studied ILs was added to solutions. However, since ILs (C2mim-Cl and C4mim-Cl) were in solid phase at room temperature, (because their melting point is around 70 ºC), mass equivalent to 1 vol.% of IL (determined using the density of ILs at their melting point) was added to the solution. 50 mL of electrolyte was used for electrochemical measurements. The used potentiostat (EG&G Princeton Applied Research Potentiostat/Galvanostat 273A) was handled by PowerSuite software. In the electrochemical cell, the working electrode was a Pt foil (Pt foil (Metrohm 6.0305.100), surface area: 1 cm^2), the reference electrode was a calomel electrode with 3.5 M KCl (HANNA instruments HI5412, 3.5 M KCl), and the counter electrode was a Pt mesh with 50 cm^2 surface area***. All potentials are converted to potential vs. reversible hydrogen electrode, RHE****.* Both HER and OER measurements were performed without adding IL and then with the addition of IL.

For HER, cyclic voltammetry (CV) was performed 2 times with 3 consecutive cycles from -0.176 V to 1.517 V at 25 mV s^{-1}. Then chronoamperometry (CA) was performed at -0.183 V for 3 min. After that linear scan voltammetry (LSV) was performed from OCP to -0.383 V at 2 mV s^{-1} at 25 ºC, 40 ºC, 50 ºC, 60 ºC, 70 ºC and 80 ºC. Finally, stability test was performed as CA at potential of -0.283 V for 7200 s at 25 ºC as well as at 80 ºC. The solutions were saved for FTIR analysis.

For OER, cyclic voltammetry (CV) was performed 2 times with 3 consecutive cycles from -0.117 V to 2.117 V at 25 mV s^{-1}. After that linear scan voltammetry (LSV) was performed from OCP to 2.117 V at

2 mV s^{-1} at 25 ºC, 40 ºC, 50 ºC, 60 ºC, 70 ºC and 80 ºC. Finally, stability test was performed as CA at potential of 1.917 V for 7200 s at 25 ºC as well as at 80 ºC. The solutions were saved for FTIR analysis.

2.4. Volume measurements

With the IL whose addition lead to the best HER and OER performance, the generated gas volume measurement was done by a Ritter Miligascounter. The electrodes were Ni electrodes with the surface area of 22.4 cm^2 for each electrode. 150 mL of 8M KOH solution with 1 vol.% of IL added were filled in an air sealed plastic beaker. The applied current of 0.8 A was controlled by the potentiostat for 2 hours.

Chapter 3. Results and Discussion

3.1. Degradation of the studied ILs

During the LSV test at different temperatures – from 25 ºC to 80 ºC – the degradation of ILs was detected. Over 40 ºC the solution started to turn to foggy white or yellow, then it turned to an opalescent orange and red. Finally, the solution holds the red colour, but it cleared out, and dark red oil like droplets were formed at the top of the solution. The process of degradation is shown below in **Figure 7**):

T / ºC	C2	C4	C1OC2	C2OC2
25				
40				
50				
60				
70				
80				
After stab.	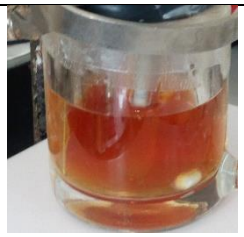			

Figure 7. *Colorization effect of the 4 different type of ILs caused by the increase of the temperature during the several LSV measurements and after the 80 ºC stability test.*

3.2. HER studies

Although the main aim of the experiment was to investigate the catalytic performance of the mentioned ILs on OER, but because the other studies on HER were related to these ILs were missing, the investigation of HER was adequate in order to evaluate the overall catalytic performance on alkaline water splitting.

3.2.1. Cyclic voltammetry measurements

Cyclic voltammetry (CV) was performed 2 times with 3 consecutive cycles from -0.176 V to 1.517 V at 25 mV s^{-1} on Pt working electrode in 8M KOH solution, with and without the addition of the ILs.

The pure 8M KOH solution shows small oxidation reaction, before HER starts to occur. This small oxidation bump was observed by other colleagues in the lab using the same Pt working electrode, and it is related to Pt oxidation (see **Figure 8A**). The addition of the ILs, significantly increased the cathodic currents recorded at -0.2 V (-3.8 mA for pure KOH; -10.2 mA for C2; -9.7 mA for C4; -11.7 mA for C1OC2; -9.8 mA for C2OC2) (see **Figure 8F**) and the onset potential for the HER (assuming -1 mA as the reference current value of the start of the reaction) was shifted to lower overpotentials (-0.119 V for pure KOH; -0.03 V for C2; 0.014 V for C4; -0.029 V for C1OC2; -0.036 V for C2OC2) (see **Figure 8G**). ILs with similar functional groups (alkyl groups C2, C4 and ethoxy groups C1OC2, C2OC2) showed similar curves (see **Figure 8G**).

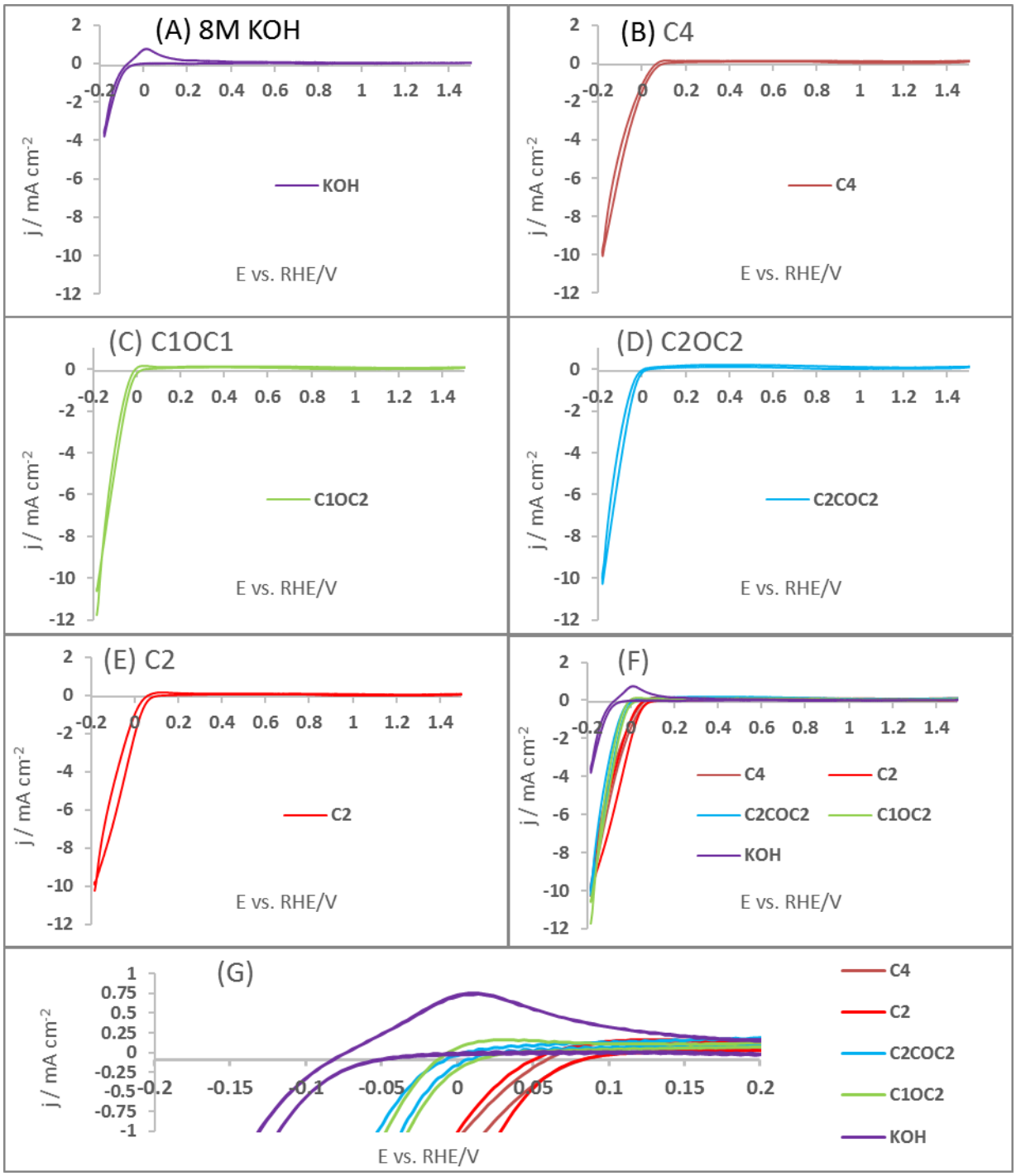

Figure 8. *Cyclic voltammetry (CV) curves of HER were recorded in duplicate with 3 consecutive cycles from -0.176 V to 1.517 V at 25 mV s^{-1}. The second cycles are shown for (A) pure 8M KOH; (B) C4 IL; (C) C1OC2 IL; (D) C2OC2 IL; (E) C2 IL; (F) Comparison of the four ILs with the pure 8M KOH solution; (G) Comparison of the onset potential of the solutions containing each of the four ILs with the pure 8M KOH solution.*

3.2.2. Linear Scan Voltammetry

KOH

The peak currents are increasing according to the temperature, however the curve belonging to 80 ºC was not parallel with the previous ones and the HER started later (see **Figure 9A**). Therefore, at lower potential lower currents were measured comparing to results of 60 ºC and of 70 ºC.

C1OC2

When the current is only the function of potential and temperature if the composition of the solution is stable, the curves should look similar as in the result of KOH. However, the polarisation curves are not following the rising of temperature, the rising of temperature from 25 ºC to 40 ºC involved the increase of currents. Then even though the temperature was rising, the currents dropped down. The lowest currents were measured at 50 ºC. After the temperature rising induced the rise of currents, but even on 70 ºC the currents were lower than at 40 ºC, and finally the highest currents measured at 80 ºC. This should indicate that the composition of the solution is changing by time, which is confirmed by the colorization of the solution, which is explained by the decomposition of the ILs (see **Figure 9C**).

C2OC2 The polarisation curves similarly to C1OC2 IL, are not following the rising of temperature, and above 25 ºC lower currents were detected at 40 ºC, 50 ºC, 60 ºC. This should indicate again, the decomposition of the IL, and indicate that the by-products of the decomposition have a negative effect on HER. At 70 ºC and 80 ºC the results are very similar (see **Figure 9D**).

C2 It seems that the decomposition of ILs have a negative effect on the HER, and the temperature rising has a positive effect on HER. In the previous measurements, it seemed that below 70 ºC the negative effect higher than the positive from the temperature rising, as in with C1OC2 and C2OC2 addition at 25 ºC the results were better than at 50 ºC and 60 ºC. But in the case of C2 the higher temperature resulted in higher currents. The increasing is not that high as in the case of pure KOH. This can be explained, by the observations of Gao et al., where they found that the shorter the chain-length on the imidazolium^{+} ring the more stable the IL is [37]. Therefore, probably the C2 IL, degradants slower hence the negative effects are lower than the positive effects from the temperature rising, and the polarisation curves of C2 added solution are parallel with pure KOH results (see **Figure 9E**).

With C4 IL, the 40 ºC curve dominates the other temperature curves. The 25 ºC curves is slightly lower (see **Figure 9B**).

Comparing the catalytic effect of ILs at 25 ºC, it can be stated that each of them catalyzes HER at 25 ºC. According to the results the most effective ILs are the following in ascendant order: C4 < C2OC2 < C1OC2 < C2 (see **Figure 9F**).

Comparing the catalytic effect of ILs at 80 ºC it appears that except the C4 IL every other performed better, than the pure KOH solution, their performance are the following in ascendant order: C4 < C2OC2 < C1OC2 < C2 (see **Figure 9G**). However, the order is similar to at 25 ºC.

Every added IL enabled the HER to start earlier, i.e., at more positive potentials (see **Figure 9H**). However, the gradient in case of C4 is much smaller than in pure 8M KOH solutions, hence smaller currents were measured. Even though a negative effect of the decomposition of ILs was noticed by the rising of temperature, higher currents were measured with C2OC2, C1OC2, C2 ILs comparing to 8M KOH at 80 ºC. The OCP was shifted to more positive potentials (see **Table 3**), after the addition of each IL. It is not clear that this more positive OCP is connected directly to the HER, or if the ILs participate in other reactions.

Table 3. *Comparison of the OCP of Pt in the KOH solution at 25 ℃ and at 80 ℃*

OCP vs. RHE/V		
	25 °C	80 °C
KOH	-0.093	-0.085
C1OC2	0.022	0.017
C2OC2	0.013	-0.036
C2	0.087	0.121
C4	0.080	0.112

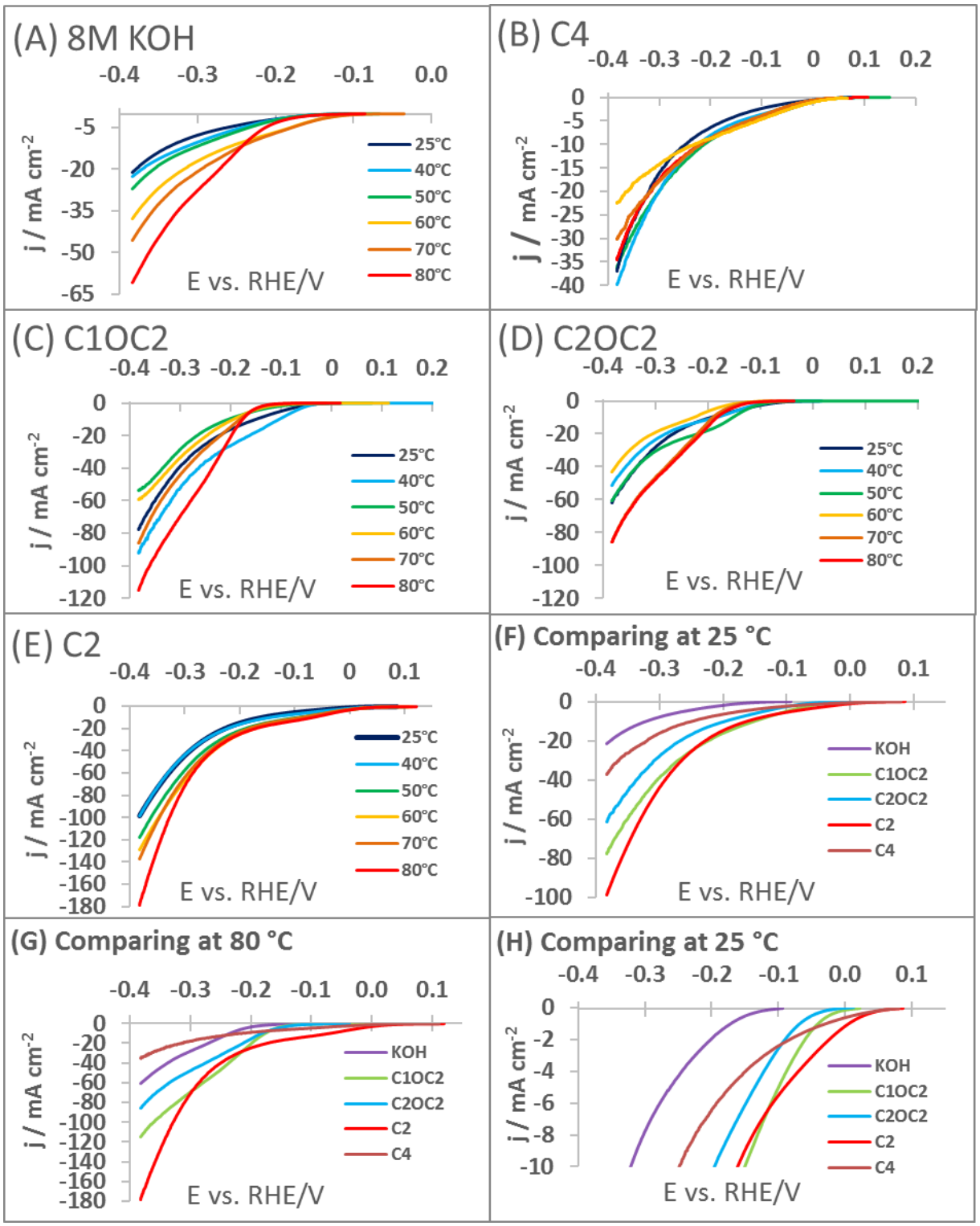

Figure 9. *Linear scan voltammetry (LSV) of HER performed from OCP to -0.383 V at 2 mV s^{-1} at 25 °C, 40 °C, 50 °C, 60 °C, 70 °C and 80 °C in IL-free 8M KOH electrolyte and with the addition of four different ILs. (A) pure 8M KOH; (B) C4 IL; (C) C1OC2 IL; (D) C2OC2 IL; (E) C2 IL; (F) Comparison of the four ILs with the pure 8M KOH solution at 25 °C; (G) Comparison of the four ILs with the pure 8M KOH solution at 80 °C; (H) Comparison of the onset potential of the four ILs with the pure 8M KOH solution.*

3.2.3. Tafel plots

In **Figure 10A** by increasing temperatures all the curves are moved to higher current densities as expected. Besides, at higher temperature, lower overpotential is needed to reach the same current density. The data related to HER in pure 8M KOH is shown in **Table 4.** The slope is over 0.120 V dec^{-1}, which indicates that the rate-determining step (RDS) is the first electron transfer reaction, which is the Volmer reaction. In **Table 4** the j_0 is increasing by the temperature, E_{10} is decreasing by temperature as expected. The j_{150} values should have increase by temperature, however our measurements were discordant to the expectations (see **Figure 10**).

C2 IL slightly increased the slope meanwhile other ILs increased it further. Generally, the addition of every ILs resulted in higher j_0, lower E_{10}, and higher j_{150} (see **Table 5 and 6**) But among those the C2 results are outstanding by their consistent performance, which means the C2 results have minor fluctuations, meanwhile other ILs shows alternating data, they reach their peak performance around 40 ºC (see **Figure 10**), as it shown in the polarization curves.

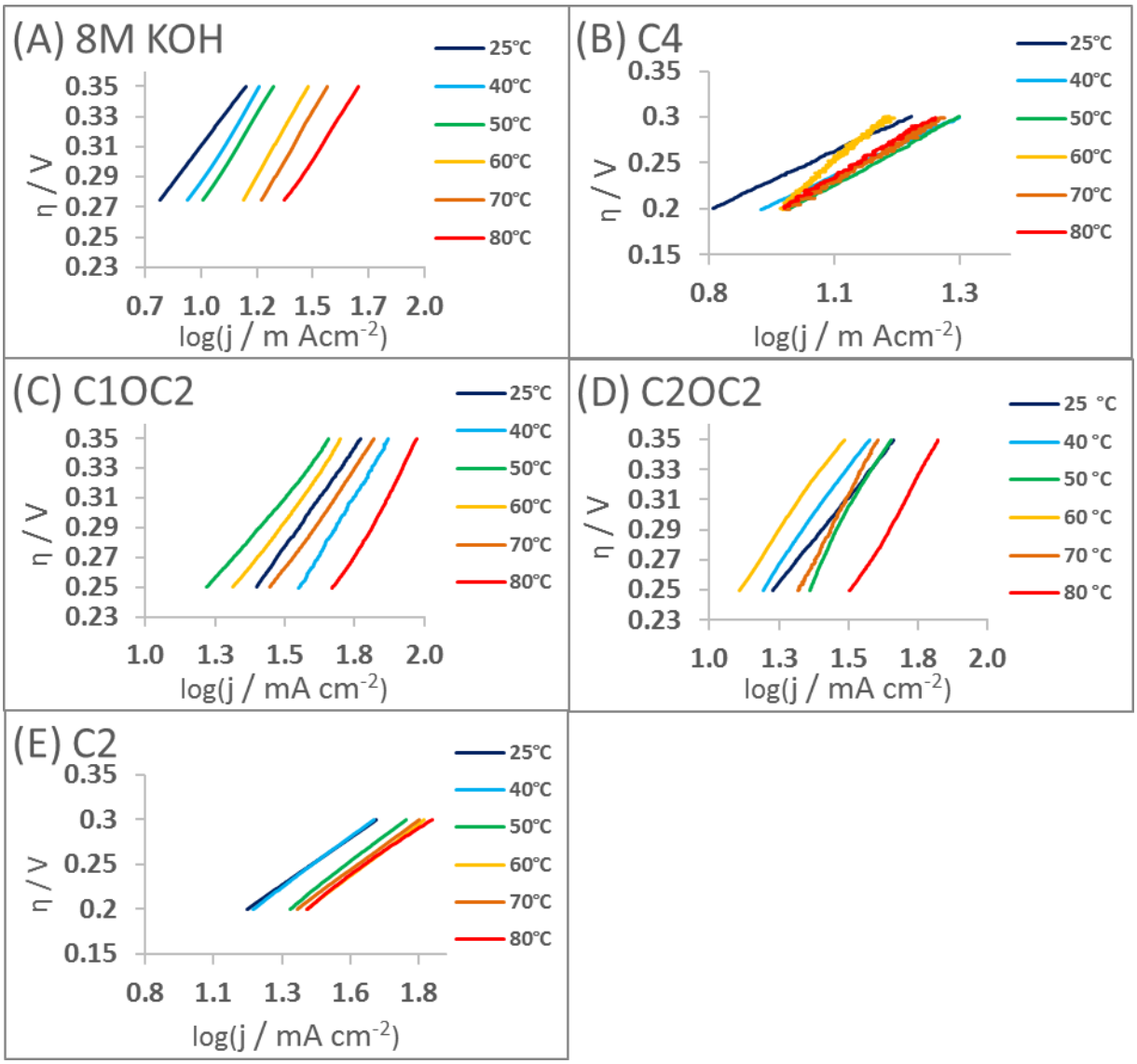

Figure 10. *Effect of temperature on Tafel slope of HER in: (A) pure 8M KOH; (B) C4 IL; (C) C1OC2 IL; (D) C2OC2 IL; (E) C2 IL.*

At 25 °C each ILs enhanced HER, meanwhile at 80 °C the addition of C4 IL did not enhance HER(see **Figure 11A**), but the addition of other ILs resulted in better HER performance (see **Figure 11B**).

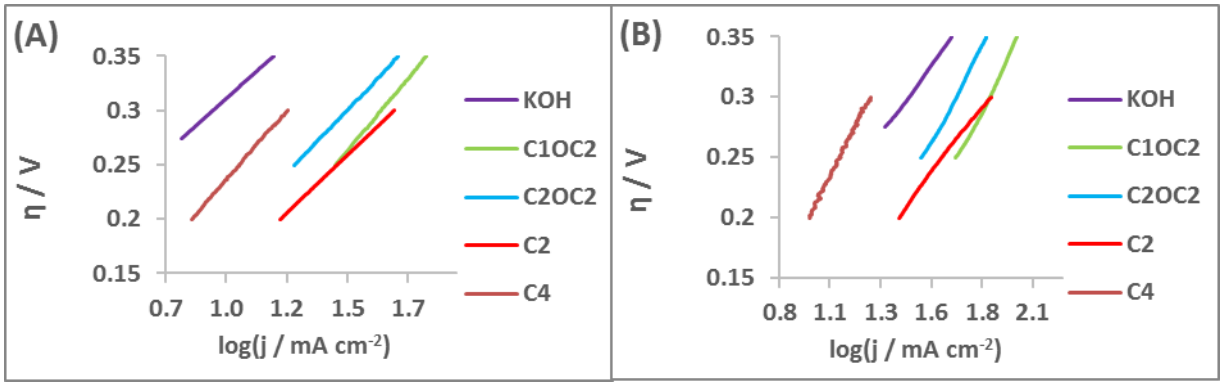

Figure 11. *Comparison of the Tafel plots of HER (A) at 25 ℃ and (B) at 80 ℃.*

Table 4. *Effect of the temperature on the Tafel regions for the HER in the electrolytes containing C2, C4, C1OC2 and C2OC2.*

8M KOH

T / ºC	Tafel slope / V dec^{-1}	j_0 / mA cm^{-2}	E_{10} / mV	j_{150} / mA cm^{-2}
25	0.198	0.2	321	0.5
40	0.234	0.5	297	0.5
50	0.243	0.7	283.5	0.5
60	0.258	1.2	238.4	2.5
70	0.256	1.4	229.4	2.5
80	0.234	1.5	235.9	0.6

C2

T / ºC	Tafel slope / V dec^{-1}	j_0 / mA cm^{-2}	E_{10} / mV	j_{150} / mA cm^{-2}
25	0.210	1.7	161	9.0
40	0.227	2.1	148	10.1
50	0.233	2.9	97.7	14.4
60	0.230	3.3	84.2	16.4
70	0.223	2.9	91.5	14.9
80	0.218	2.9	70.7	16.9

C4

T / ºCº	Tafel slope / V dec^{-1}	j_0 / mA cm^{-2}	E_{10} / mV	j_{150} / mA cm^{-2}
25	0.254	1.0	248	4.0
40	0.257	1.3	224	5.3
50	0.295	1.9	211.7	6.3
60	0.460	3.2	227.0	6.8
70	0.313	2.0	216.5	6.0
80	0.332	2.2	220.5	6.5

C1OC2

T / ºCº	Tafel slope / V dec^{-1}	j_0 / mA cm^{-2}	E_{10} / mV	j_{150} / mA cm^{-2}
25	0.265	2.9	150	9.9
40	0.313	5.7	104	17.8
50	0.226	1.3	204.2	4.7
60	0.257	2.2	194.0	4.0
70	0.267	3.3	181.6	3.5
80	0.338	8.8	176.2	3.3

C2OC2

T / ºCº	Tafel slope / V dec^{-1}	j_0 / mA cm^{-2}	E_{10} / mV	j_{150} / mA cm^{-2}
25	0.229	1.4	195	6.2
40	0.262	1.7	184	6.4
50	0.341	4.1	152.0	9.5
60	0.272	1.5	225.8	1.7
70	0.359	4.2	207.7	1.8
80	0.323	5.6	182.8	3.8

Table 5. *Comparison of the kinetic parameters of HER after the addition of 4 different IL at 25 ºC.*

at 25 ºC	Tafel slope / V dec^{-1}	j_0 / mA cm^{-2}	E_{10} / mV	j_{150} / mA cm^{-2}
KOH	0.191	0.2	321	0.5
C1OC2	0.256	2.9	150	9.9
C2OC2	0.229	1.4	195.0	6.2
C2	0.210	1.6	161.0	9.0
C4	0.251	1.0	248.2	4.0

Table 6. *Comparison of the kinetic parameters of HER after the addition of 4 different IL at 80 ºC.*

at 80 ºC	Tafel slope / V dec^{-1}	j_0 / mA cm^{-2}	E_{10} / mV	j_{150} / mA cm^{-2}
KOH	0.241	1.5	236	0.6
C1OC2	0.379	8.8	176	3.3
C2OC2	0.323	5.6	182.8	3.8
C2	0.218	2.9	70.7	17.0
C4	0.350	2.2	220.5	6.5

3.2.4. Stability test

At 25 ºC at the beginning of the stability test, the C2 IL started at the highest current density, comparing to KOH 20 times higher. However, the high current density was jumping down rapidly, after about 3500 s the currents density of C2 got lower than the current density of KOH. The C2OC2 IL has similar ascending trend as C2, at the end of the test both of them have smaller current densities than KOH (see **Figure 12A**). The highest final current was obtained by C1OC2 IL, barely over 4 mA cm^{-2}. The C4 IL reached similar final current density as KOH, but it started, much higher, and the current density reduction was slower comparing to KOH (see **Figure 12B**).

At 80 ºC the highest starting current density was achieved by the C1OC2 and the C2OC2 ILs see **Figure 12C**).. These IL represent fast jump down as well as C2 behaved at 25 ºC. These two IL also had lower current densities than KOH by the end of the test. The C2 had higher starting current density than C4 and KOH and show a descending trend until about 4700 s, after that the current density starts to slowly increase by step by step, and show increasing trend at the end of the test. This strange increasing trend is also observed much earlier with the addition of C4, moreover the C4 made a more rapid elevation then a more rapid decreasing. The most consistent current density was achieved by C4, which dominates the stability test result after around 1000 s and has a generally increasing part until 5100 s after that it shows a descending trend until the end of the test (see **Figure 12D**). This unexpected behaviour of the stability test curves might be due to experimental error. However, the strange behaviour was found twice with the addition of C2 and C4 IL. Another explanation can be that different intermediates of the degradation of these IL liquids has different effect on the HER. The intermediates at the beginning have a slowing influence on HER, and the later intermediates have a positive effect on

HER. Also, the reactions of the IL degradation can influence the measured current density.

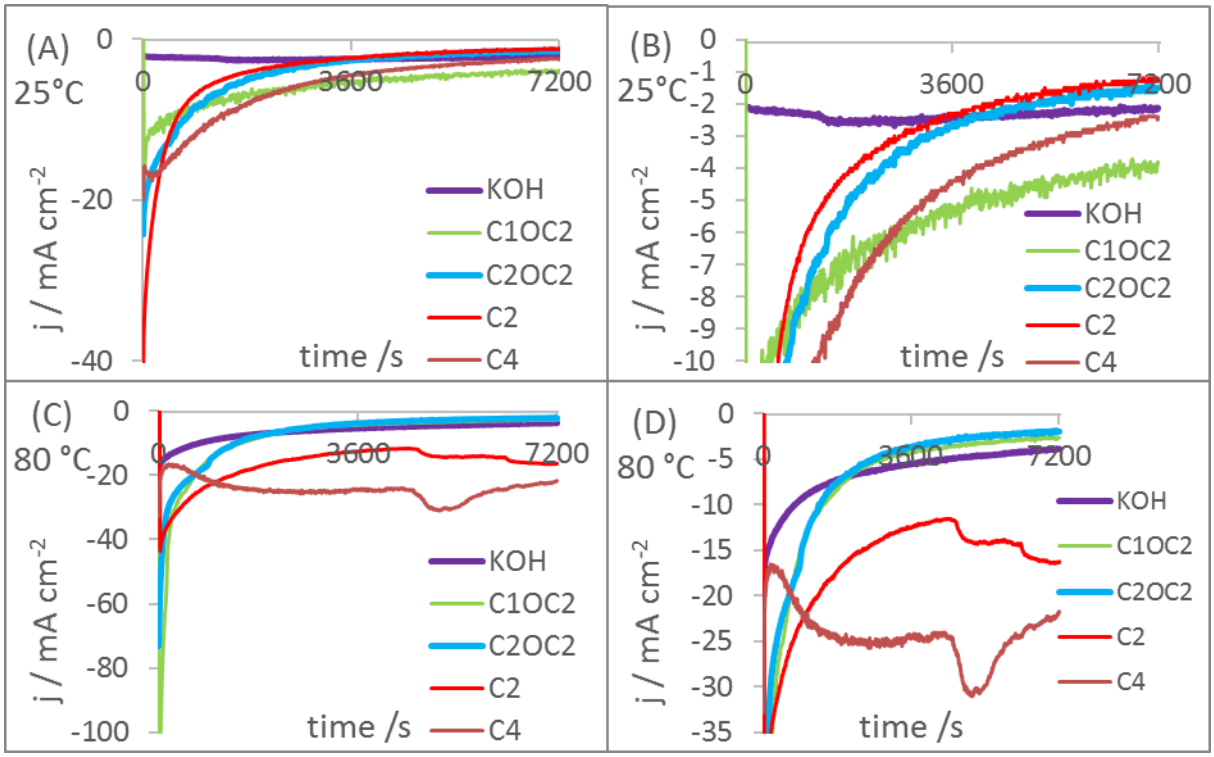

Figure 12. *2h-long HER stability test in pure 8 M KOH solution and with the addition of C1OC2, C2OC2, C2 and C4 ILs. on -0.283 V: (A) at 25 ℃ ; (B) at 25 ℃ with y axis range from 0 to 10 mA cm^{-2}; (C) at 80 ℃; (D) at 25 ℃ with y axis range from 0 to 35 mA cm^{-2}*

3.3. OER studies

3.3.1. Cyclic Voltammetry

Cyclic voltammetry (CV) was performed 2 times with 3 consecutive cycles from -0.176 V to 1.517 V at 25 mV s-1 on Pt working electrode in 8M KOH solution, with and without the addition of the ILs. The pure KOH solution has a significantly higher current density peak than C4, C1OC2 and C2OC2 ILs (see **Figure 13F**). The C1OC2 and the C2OC2 curves have very similar trends and peaks so as in the CV measures of HER. The other two ILs, C2 and C4 have very different trends and peaks. C2 also has a significantly higher peak than KOH. Because from HER CV result, we would expect again similar trends and peaks for ILs with analogs function croups (namely -ethyl and -butyl groups) see **Figure 13C,D**). Therefore, the C2 results suggest possible experimental error, which can be related to a missed preparation of the 8M KOH solution by overdosing KOH. However, because of the small number of samples of ILs, it was not possible to repeat HER and OER measurements in order to save enough IL sample for the volume measuring tests.

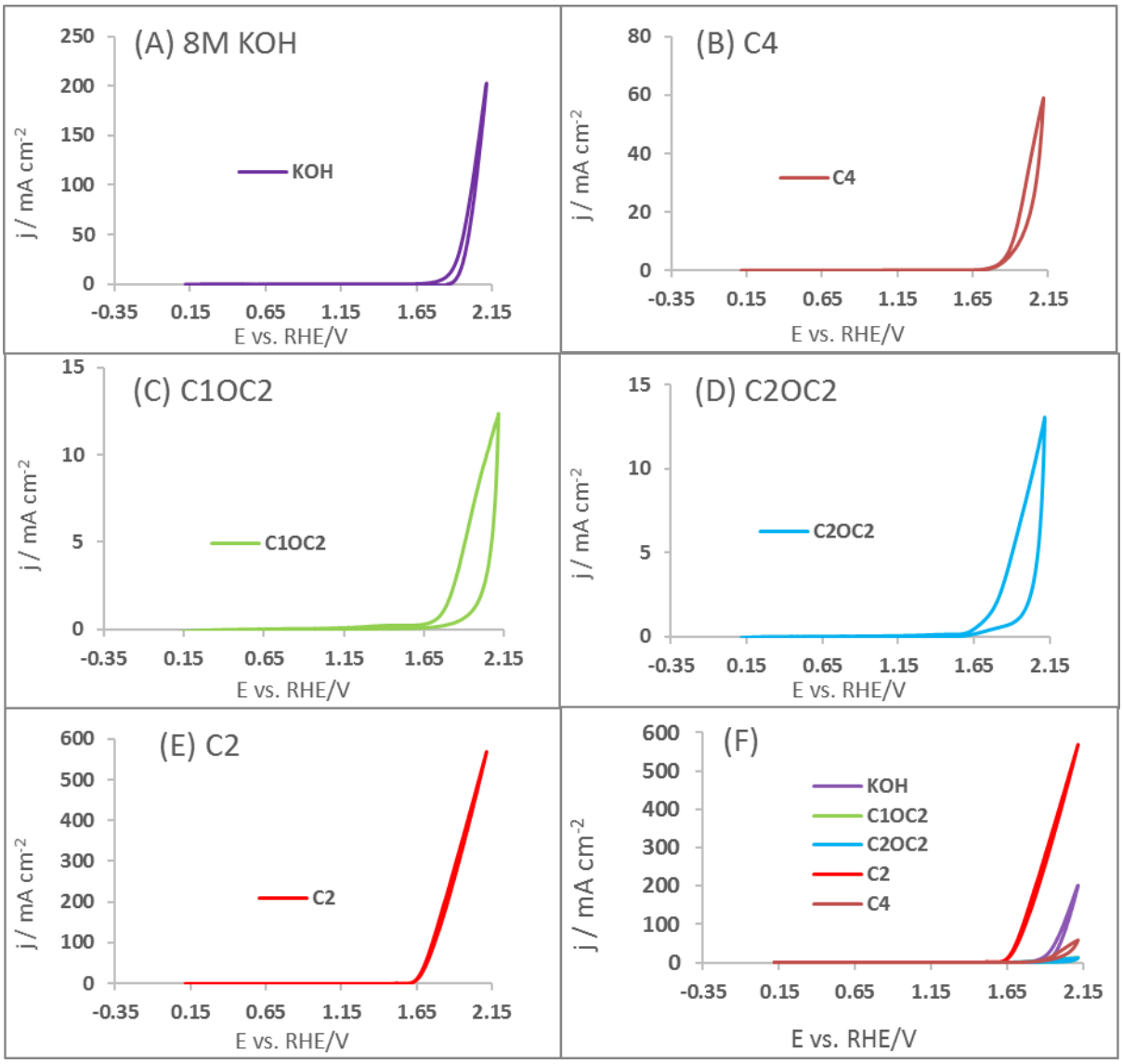

Figure 13. *Cyclic voltammetry (CV) curves were recorded 2 times with 3 consecutive cycles from 0.125 V to 2.12 V at 25 mV s^{-1}. The second cycles are shown. (A) pure 8M KOH; (B) addition of C4, (C) addition of C1OC2, (D) addition of C2OC2, (E) addition of C2, (F) Comparison of four ILs.*

3.3.2. Linear Scan Voltammetry

In the case of pure 8M KOH solution the peak currents are increasing according to the temperature rising. The curves are parallel as expected, except the 80 ºC line whereas the OER starts earlier (see **Figure 14A**). Comparing C1OC2 OER results to HER LSV results, the temperature lines are parallel, and there is no sign of the negative effect of the C1OC2 IL degradation in the case of OER, since, for higher temperatures higher currents densities were measured, similar to the KOH OER results (see **Figure 14C**). In the case of C2OC2 the effect of degradation is less, comparing to C2OC2 HER LSV experience. Although 25 ºC line starts better than 40 ºC finally got worst results than 40 ºC (see **Figure 14D**).

Contrary to C2 HER LSV experience the degradation of IL has a much more significant negative influence on OER of C2 IL . The 25 ºC current densities are higher than the at 40 ºC, 60 ºC, 70 ºC and

80ºC. The highest current density reached at 50 ºC, and surprisingly the lowest current density is measured at 70 and at 80 ºC (see **Figure 14E**).

The C4 polarisation curves are showing the negative effect of the IL degradation. The 40ºC 50ºC and 60ºC lines are under the 25 ºC line. The 70 ºC and 80 ºC lines are higher than the 25 ºC line, and their trend is similar (see **Figure 14B**).

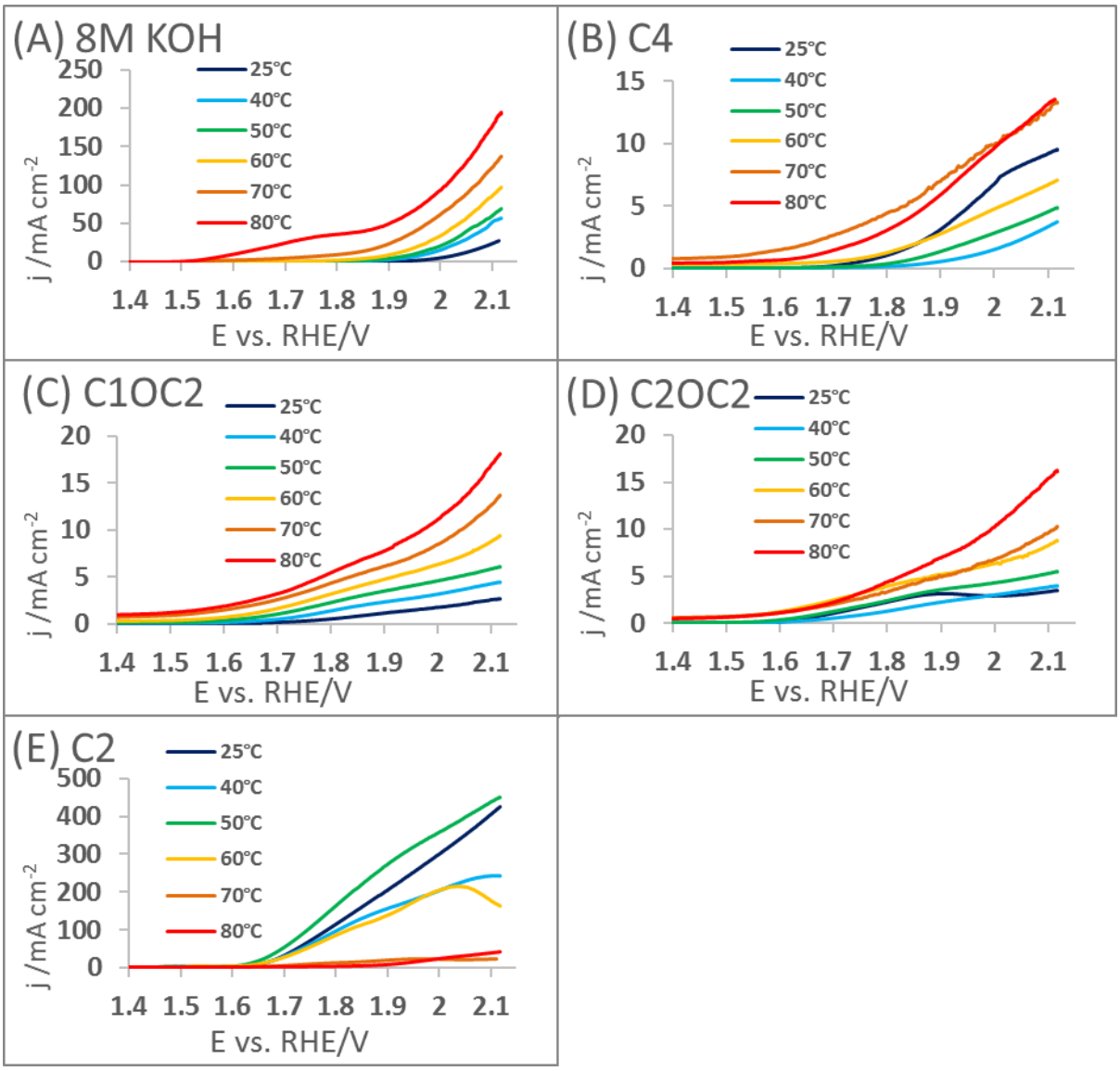

Figure 14. *Linear scan voltammetry (LSV) performed from OCP to 2.12 V at 2 mVs^{-1} at 25 ºC, 40 ºC, 50 ºC, 60 ºC, 70 ºC and 80 ºC in: (A) pure 8 M KOH; (B) in 8 M KOH with addition of C4, (C) in 8 M KOH with addition of C1OC2, (D) in 8 M KOH with addition of C2OC2, (E) in 8 M KOH with addition of C2.*

The C2 results are excessively outstanding (see **Figure 15A**), which suggests again the suspicion of experimental error. Besides that, the other ILs helped OER to start earlier (see **Figure 15B**), but on the other hand each IL slowed down the reaction, and the pure KOH solution resulted in higher current densities (see **Figure 15C**). The OCP is shifted to more negative potentials when ILs were used.

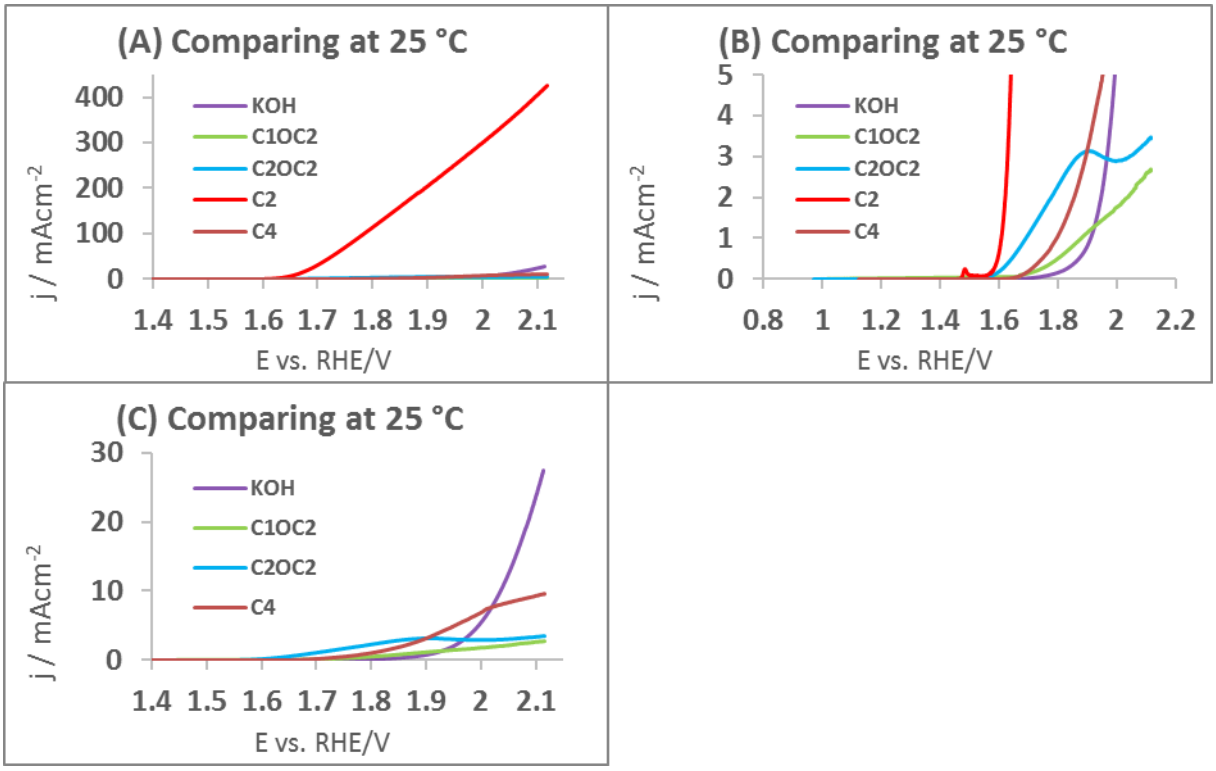

Figure 15. *Comparison of the polarisation curves of OER at 25 ºC in pure 8M KOH solution, and the addition of four different types of ILs. (A) comparison of all solutions; (B) Comparison of reaction starting points; (C) Exclusion of C2 data for better overlook of other results.*

At 80 ºC the negative effect of degradation using C2 IL is very remarkable (see **Figure 16A**), because at 25 ºC it produces around 400 mA cm^{-2}, which dropped down to around 50 mA cm^{-2}. This result is four times smaller comparing to the KOH results at 80 ºC. Other ILs show even lower current densities than C2 (see **Figure 16C**). The OCP shifting towards more negative potentials, at high temperatures is more noticeable (see **Figure 16B** and **Table 7**).

Table 7. *Comparison of the OCP of the different solutions at 25 ºC and at 80 ºC*

	OCP vs. RHE/V	
	25 °C	80 °C
KOH	1.518	1.305
C1OC2	0.984	0.479
C2OC2	0.973	0.538
C2	1.282	0.483
C4	1.125	0.510

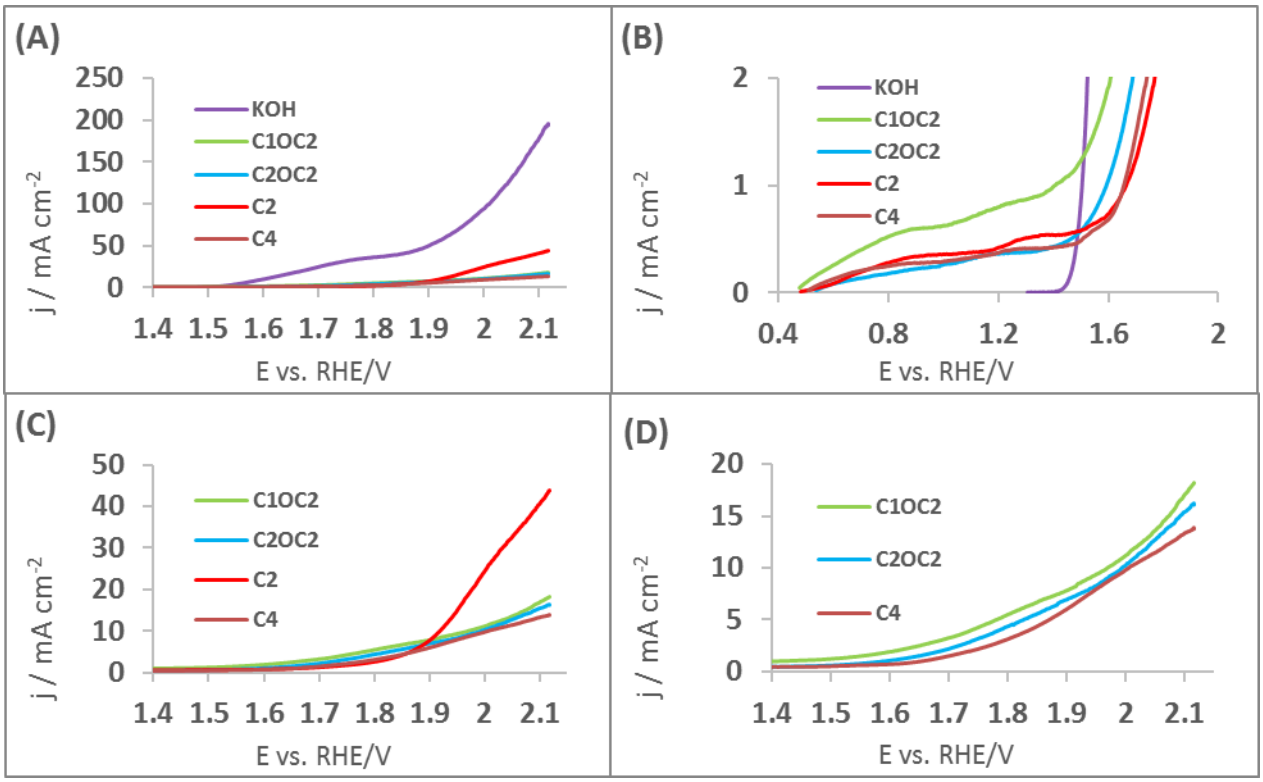

Figure 16. *Comparison of polarisation curves of OER at 80 ºC in pure 8M KOH solution, and the addition of four different types of ILs. (A) comparison of all solutions; (B) Comparison of reaction starting points; (C) Excluding KOH data for better overlook of other results; (D) Excluding KOH and C2 data for a better overview of the other results.*

3.3.3. Tafel plots

In pure KOH solution during OER the curves are shifted to higher currents by increasing the temperature as it was expected (see **Figure 17A**). Comparing to the HER, higher overpotentials were needed to reach linear region of Tafel plots (shown in **Figure 17**). Comparing the OER Tafel slopes in pure KOH solutions to HER, it appears that below 80 ºC the slopes are smaller, but at 80 ºC the slope is around twice as big, respectively 0.457 V dec^{-1}. At other temperatures, it is increasing from 0.133 V dec^{-1} at 25 ºC to 0.219 V dec^{-1} at 70 ºC (see **Table 8**). This value is also higher than 0.120 V dec^{-1} which indicates that the RDS is the first electron transfer reaction which is the Volmer reaction likewise as it was shown during HER. In pure KOH, the j_0 values are increasing by temperature, E_{01} values are decreasing by temperature and the j_{500} values are increasing by temperature as was expected (see **Table 8**).

Each IL increased the slope, at each temperature, except C2 and C4 at 80 ºC. Each IL increased j_0 at the temperature range from 25 ºC to 60 ºC. At higher temperatures, the j_0 values are dropped down, and at 70 ºC they are still higher than the KOH results, but at 80 ºC the addition of ILs decreasing j_0 (see **Table 8**). At 25 ºC each ILs reduced the E_{01} value (see **Table 9**). Below 70 ºC, in general, they are reducing further the E01, but above 70 ºC only C1OC2 IL reduced the E01. According to j_{500} the ILs have a similar effect on OER, which means they have a catalytic effect under 70 ºC, and at 80 °C they performed worse (see **Table 10**).

Table 8. *Effect of the temperature on the Tafel regions for the OER in the electrolytes containing C2, C4, C1OC2 and C2OC2.*

KOH

T / ºC	Tafel slope / V dec^{-1}	j_0 / mA cm^{-2}	E_{01} / mV	j_{500} / mA cm^{-2}
25	0.133	8.8E-06	674	0.1
40	0.145	8.9E-05	586	0.2
50	0.153	2.4E-04	551	0.4
60	0.161	7.4E-04	492	1.1
70	0.219	0.02	292	6.7
80	0.457	1.8	263	30.6

C2

T / ºCº	Tafel slope / V dec^{-1}	j_0 / mA cm^{-2}	E_{01} / mV	j_{500} / mA cm^{-2}
25	0.487	9.0	369	62.1
40	0.674	16.3	248	53.4
50	0.573	19.1	216	93.4
60	0.540	8.4	265	47.4
70	0.492	0.9	390	7.8
80	0.180	0.002	425	1.6

C4

T / ºCº	Tafel slope / V dec^{-1}	j_0 / mA cm^{-2}	E_{01} / mV	j_{500} / mA cm^{-2}
25	0.231	4.3E-03	616	0.4
40	0.186	1.5E-04	792	0.06
50	0.210	9.7E-04	706	0.2
60	0.334	0.03	615	0.7
70	0.491	0.3	410	3.3
80	0.370	0.1	500	2.0

C1OC2

T / ºCº	Tafel slope / V dec^{-1}	j_0 / mA cm^{-2}	E_{01} / mV	j_{500} / mA cm^{-2}
25	0.364	0.02	640	0.2
40	0.606	0.2	525	0.8
50	0.676	0.4	456	1.5
60	0.681	0.5	401	2.2
70	0.788	0.9	276	3.2
80	0.693	0.9	169	4.0

C2OC2

T / ºCº	Tafel slope / V dec^{-1}	j_0 / mA cm^{-2}	E_{01} / mV	j_{500} / mA cm^{-2}
25	1.405	1.0	453	1.6
40	0.551	0.1	521	0.8
50	0.838	0.6	431	1.7
60	1.025	1.2	336	3.0
70	0.736	0.6	345	2.5
80	0.560	0.5	353	2.9

At 25 ºC the addition of each ILs increased the slope. The highest increment was done by C2OC2 almost 10 times higher, the lowest increment was done by C4 which almost doubled the slope. Every ILs increased j_0, similarly as in HER, but during OER the increment is more significant. Each ILs decreased the E_{01}, the reduction was minor in connection with C4 and C1OC2 ILs, meanwhile the C2OC2 reduced E_{01} by 33%, and the C2 reduced it by 45%. Each ILs significantly rose j_{500} current density (see **Table 10**). At 80 ºC the slope was reduced only by C2. Each ILs reduced j_0, C2 the most. The E_{01} was reduced only by C1OC2 and none of the ILs increased j_{500}, whereas C2 performed the worst (see **Table 11**). The comparison of Tafel diagrams at 25 ºC and at 80 ºC are shown in **Figure 18**.

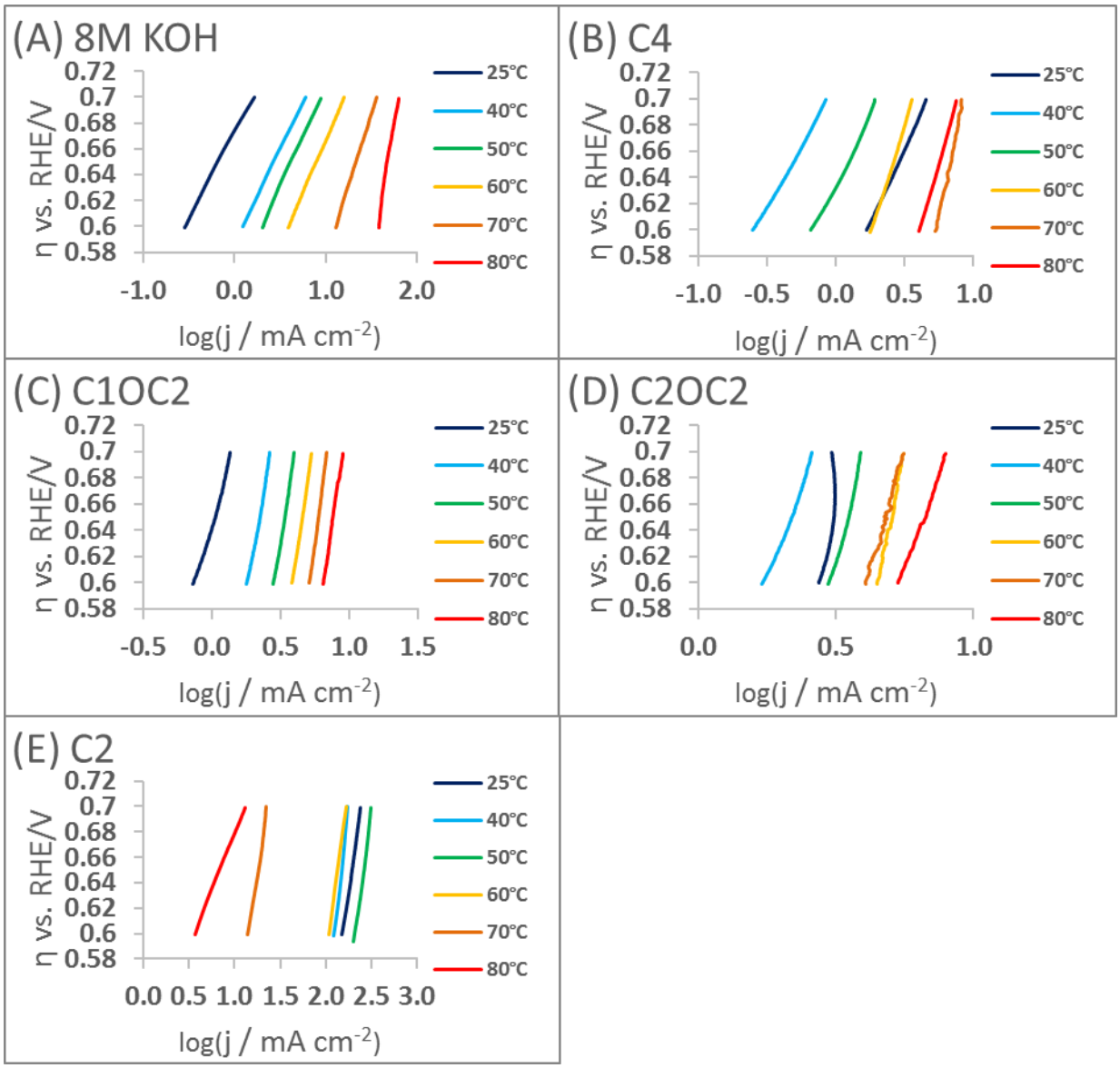

Figure 17. *Effect of temperature on Tafel slopes of OER in: (A) pure 8M KOH; and after addition of (B) C4 IL; (C) C1OC2 IL; (D) C2OC2 IL; and (E) C2 IL.*

Table 9. *Comparison of kinetic parameters of OER after the addition of 4 different IL at 25 ºC*

at 25 ºC	Tafel slope / V dec^{-1}	j_0 / mA cm^{-2}	E_{01} / mV	j_{500} / mA cm^{-2}
KOH	0.133	8.8E-06	674	0.06
C1OC2	0.364	0.02	640	0.2
C2OC2	1.405	1.1	453	1.6
C2	0.487	9.0	369	62.1
C4	0.231	4.3E-03	616	0.4

Table 10. *Comparison of kinetic parameters of OER after the addition of 4 different IL at 80 ºC*

at 80 ºC	Tafel slope / V dec^{-1}	j_0 / mA cm^{-2}	E_{01} / mV	j_{500} / mA cm^{-2}
KOH	0.457	1.8	263	30.6
C1OC2	0.693	0.9	169	4.0
C2OC2	0.560	0.5	353	2.9
C2	0.180	0.002	425	1.6
C4	0.370	0.1	500	2.0

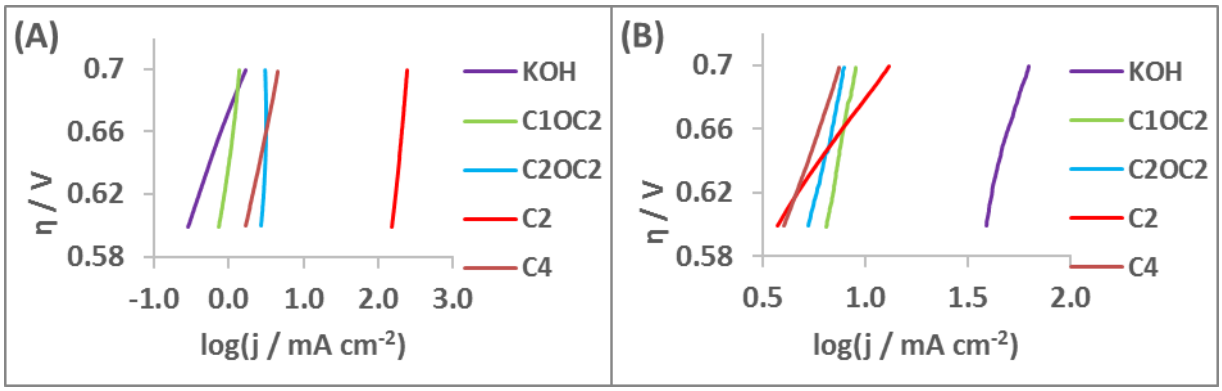

Figure 18. *Comparison of OER Tafel plots at 25ºC and at 80ºC.*

3.3.4. Stability test

During the stability test at 25 ºC the C2 IL performed outstandingly the best (see **Figure 19A**), therefore in **Figure 19B** the C2 data was taken away to facilitate the comparison. Among the other ILs C4 performed the best having much higher current densities than C1OC1 and C2OC2. C4 curve shows an ascending trend which is not in accordance with the expectations, and still shows lower current densities than KOH. KOH has a descending trend as expected. For further comparison, KOH and C2 data were taken away again. C1OC2 and C2OC2 ILs show very small current densities, in general lower than 0.5 mA. Among them, C1OC2 performed better, and each ILs show a descending trend. At 80 ºC none of the ILs facilitated OER, even more the addition of ILs are resulted in at least 3 times lower current densities. The KOH curve has an unexpected increasing trend in the beginning, and it slightly started to ascend just in the second half of the experiment (see **Figure 20A**). For better comparison, KOH data were taken away. Among ILs C2 performed the best, which was followed by C1OC2 IL. Each curve has an ascending trend, C2 has a square root shape, meanwhile C1OC2 has a square shape (see **Figure**

20B). These ILs highly overperformed C4 and C2OC2. C4 and C2OC2 have similar ascending trends and amplitude. Each IL curves have an ascending trend, which was unexpected (see **Figure 20C**).

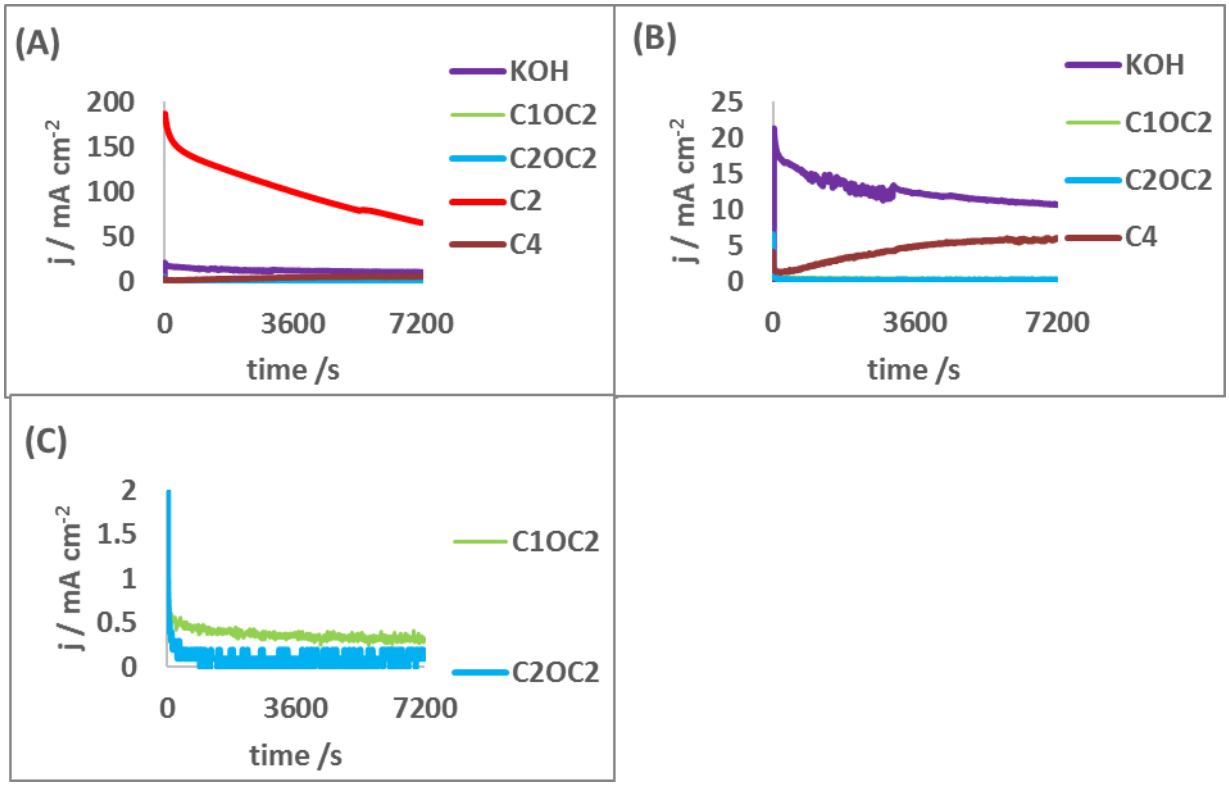

Figure 19. *2h long OER stability test on 1.92 V at 25 ℃ (A) pure 8M KOH solution with the addition of C1OC2, C2OC2, C2 and C4 ILs; (B) Excluding C2 data for better overlook of other results; (C) Excluding KOH, C2 and C4 data for better overview of other results.*

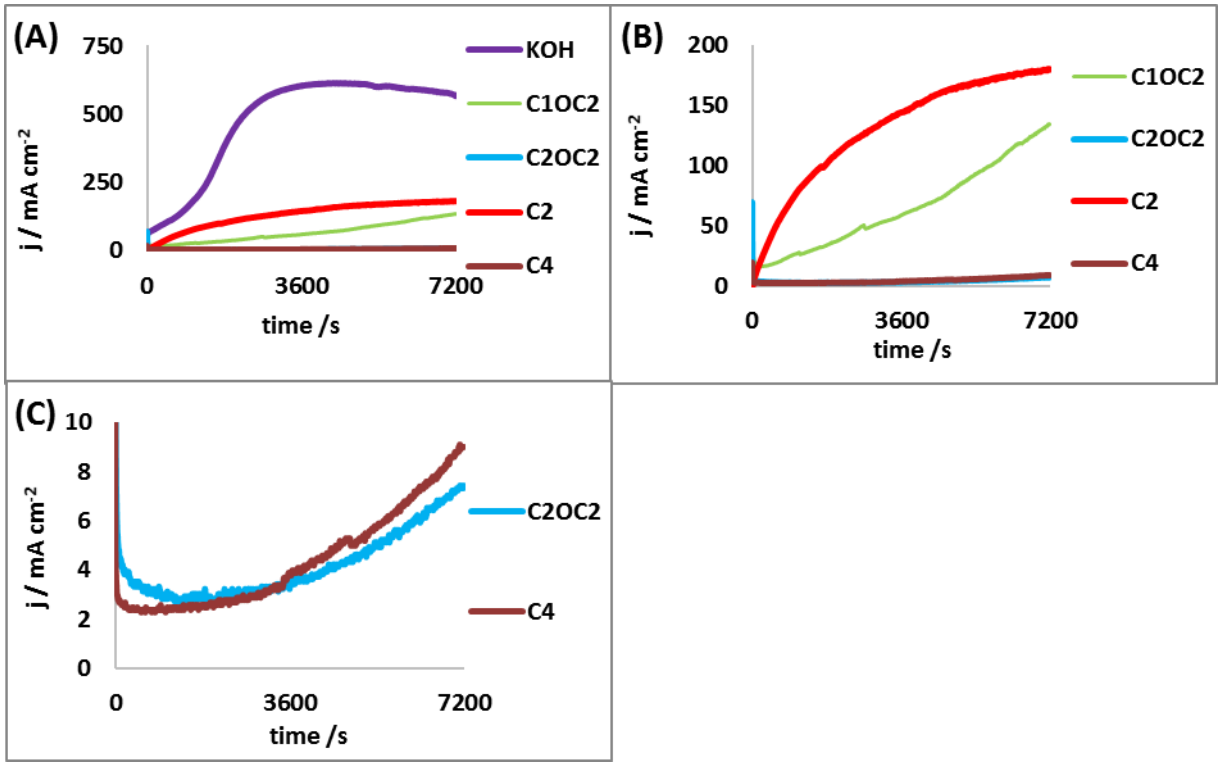

Figure 20. *2h long OER stability test on 1.92 V at 80 ℃ (A) pure 8M KOH solution with the addition of C1OC2, C2OC2, C2 and C4 ILs; (B) Excluding KOH data for better overlook of other results; (C) Excluding KOH, C2 and C1OC2 data for better overview of other results.*

3.4. Summary of fundamental measurements

For the volume measurements, evaluating the performance of the ILs and chose the best one was needed. However, there were no ILs that unequivocally outperformed the others. Although during the OER experiments, the outstanding results of C2 suggest the possibility of experimental error, in case of the lack of samples to repeat the C2 OER measurements, finally we chose C2 as the best performing IL because of the followings:

-C2 performed the best during LSV of HER

-C2 had the highest current densities at the beginning of the HER stability tests

-C2 looks more stable comparing to other ILs according to HER data

-During LSV of OER at 25 ºC C1OC2 and C2OC2 performed the worst

-During the stability test of OER at 25 ºC C1OC2 and C2OC2 performed by far the worst as well

3.5. Volume measurements

3.5.1. Measuring method

The gas production was measured once during a 2 h long galvanostatic electrolysis using Squid Potentiostat, when constant current was applied, and secondly during a 2 h long potentiostat electrolysis when constant potential was applied.

3.5.1.1. Galvanostatic electrolysis

- Plastic cell with 150 mL of 8M KOH electrolyte (with and without the addition of 1% vol. of C2mim)
- Ni electrodes, both for anode and cathode
- Chronopotentiometry (CP) run at 0.8 A.
- Measurement of the gas volume (with Ritter) released during electrolysis
- Experiment run for 2 hours or until the potential reaches 2.9 V. Set cut-off potential to 2.9 V (this means that the experiment is interrupted if the cell potential gets higher than 2.9 V).

Previously 0.35 g C2mim was used twice for HER and OER test for 50 mL of 8M KOH solution. Therefore, for 150 mL of KOH solution 3 times 0.35g (1.05 g) C2mim were used.

3.5.1.2. Potentiostat electrolysis

The same approach was carried out in Squid Potentiostat but using a constant potential of 2.3 V.

A linear sweep of the potential, from 1.5 V to 2.3 V, at 100 mV s^{-1} scan rate is done to avoid high current jumping at the beginning because the squid potentiostat can handle currents only up to 1 A.

3.5.1.3. Calculations

- **Total energy used during the test:**

During the tests, the current (I / A) and the potential (U / V) were measured. From these data, the power (P / W) was obtained at each sample time as **eq. (30,31)**:

$$I_0 \cdot U_0 = P_0 \,/W \tag{30}$$

$$\frac{799.7\ [mA]}{1000} \cdot 2.19\ [V] = 1{,}75\ [W] \tag{31}$$

The corresponding at time 0 / s and at time 5 / s, shown in **Table 11**:

Table 11. *First 2 sample point of CP of KOH solution to explain the calculations*

Elapsed Time (s)	Working Electrode / V	Current / mA	Power / W	Δ_{charge} /C	Δ_{energy} /J
0	2.19	799.70	1.75	0	0
5	2.21	799.71	1.77	4.00	8.81

The total amount of energy used during the test was calculated by integrating the obtained power-time chart by the time with the trapezoidal rule – shown in **Figure 21** - **see eqs (32-35)**:

$$E[J] = \int_{t0=0}^{t1438=7193} P(t) \cdot dt \approx \sum_{i=1}^{1438} \frac{P(t_{i-1}) + P(t_i)}{2} \cdot (t_i - t_{i-1}) = \sum_{i=1}^{1438} \Delta E_i \tag{32}$$

$$\Delta E_i = \frac{P(t_{i-1}) + P(t_i)}{2} \cdot (t_i - t_{i-1}) \tag{33}$$

$$\Delta E_1 = \frac{P(t_0) + P(t_1)}{2} \cdot (t_1 - t_0) = \frac{1.75 + 1.77}{2}(5 - 0) = 8.8\ [J] \tag{34}$$

$$Area = E\ [J] = \underline{14004.91\ J} \tag{35}$$

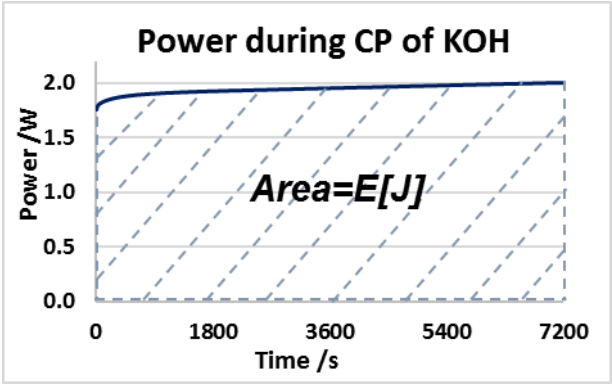

Figure 21. *Applied power on the cell*

- **Total charge during the test:**

The total amount of charge was calculated by integrating the charge-time chart by the time in the same way as the total amount of energy was calculated, **see eqs (36-39)**:

$$Q[C] = \int_{t0=0}^{t1438=7193} I(t) \cdot dt \approx \sum_{i=1}^{1438} \frac{I(t_{i-1}) + I(t_i)}{2} \cdot (t_i - t_{i-1}) = \sum_{i=2}^{1438} \Delta Q_i \tag{36}$$

$$\Delta Q_i = \frac{Q(t_{i-1}) + Q(t_i)}{2} \cdot (t_i - t_{i-1}) \tag{37}$$

$$\Delta Q_1 = \frac{I(t_0) + I(t_1)}{2} \cdot (t_1 - t_0) = \frac{0{,}7997 + 0{,}79971}{2}(5 - 0) = 4.00[C] \tag{38}$$

$$Q = \underline{5753.02\ C} \tag{39}$$

- **Theoretical produced gas volume:**

The theoretical volume of the produced gas was calculated by the total charge that went through the cell, from where we can calculate the moles of electrons that passed through the cell (see **eq. (40)**):

$$n_e = \frac{\frac{Q}{q_e}}{N_A} = \frac{\frac{5753.02\ [C]}{1.602176634 \cdot 10^{-19}\ [\frac{C}{e^-}]}}{6.0221409 \cdot 10^{23}\ [\frac{1}{mol}]} = 0.06\ [mol\ e^-] \quad (40)$$

where: q_e: is the elementary charge, or the charge of one electron

N_A : is Avogadro's number

Cathode (HER) (see **eq. (41,42)**):

$$2H^+ + 2e^- \rightleftharpoons H_2 \quad (41)$$

$$0.06\ H^+ + 0.06\ e^- \rightleftharpoons 0.03\ H_2 \quad (42)$$

Anode (OER) (see **eq. (43,44)**):

$$2H_2O \rightleftharpoons O_2 + 4H^+ + 4e^- \quad (43)$$

$$0{,}03\ H_2O \rightleftharpoons 0{,}015\ O_2 + 0{,}06\ H^+ + 0{,}06\ e^- \quad (44)$$

According to the HER and OER mentioned above with 1 mol electron half mole hydrogen gas and ¼ oxygen gas are produced. Summing up the total moles of gases (see **eq. (45)**):

$$n_{H^2} + n_{O^2} = n_{total} = 0{,}03 + 0{,}015 = 0{,}045\ mol\ gas \quad (45)$$

From the number of moles we can calculate the volume of the gas with the standard molar volume ((see **eq. (46)**) at STP conditions (0 ºC, 1 atm) (see **eq. (47)**):

$$V_m = 22.414[\frac{dm^3}{mol}] \quad (46)$$

$$V_{theo} = n_{total} \cdot V_m = 0{,}045 \cdot 22.414 = 1{,}009\ [dm^3\ gas]\ at\ STP \quad (47)$$

- **Resistance:**

Resistance was calculated by the average current and the average potential during the test (see **eq. (48)**):

$$R = \frac{U_{AVG}}{I_{AVG}} = \frac{2.43}{0.7997} = 3.04\ [\Omega] \quad (48)$$

- **Volume measuring:**

The MGC-1 PMMA MILLIGASCOUNTER (MGC) was used. Because the volumes only can be compared on similar conditions, the volume measured by the MGC must be recalculated to STP conditions.

Also due to the design of the MilliGascounter this overpressure of 5 mbar will remain in the dead-space volume at the end of the test. The deficit volume caused by this effect must be added to the measured/indicated volume.

The calculations are described in the manual of the MGC as follow (see **eq. (49)**):

$$V_D = V_{DS} \cdot \left(\frac{P_a + P_{DS}}{P_a} - 1\right) = 0.267 \cdot \left(\frac{1013.25 + 5}{1013.25} - 1\right) = 0.001315\ dm^3 \quad (49)$$

where: V_D = Deficit volume

V_{DS}= Dead space volume

P_a = Actual ambient pressure [mbar]

P_{DS} = Remaining pressure in dead space volume = 5 [mbar]

The dead space volume is defined as the volume of the total gas pipeline system between the gas source and the MilliGascounter (for fermentation tests: including the volume of the fermentation vessel above the substrate). In this case (see **eq. (50)**):

$$V_{DS} = \frac{d^2_{pipe\ inner} \cdot \pi}{4} \cdot l_{pipe} + V_{above\ solution} = \frac{0.04^2 \cdot 3.14}{4} \cdot 2 + 0.264 = 0.267\ dm^3 \quad (50)$$

- Effect of Water Vapour Partial Pressure:

If the measurement result must be corrected for the volumetric share of water vapour, the values in the following **Table 12**, which take the temperature into account, can be used in the equation (51) given below:

Table 12. *Data of vapour partial pressure related to temperature.*

Temp. °C	Water vapour partial pressure / mbar (psi)		Temp. / °C	Water vapour partial pressure / mbar (psi)		Temp. / °C	Water vapour partial pressure / mbar (psi)
15	17.0 (0.246)		20	23.4 (0.339)		25	31.7 (0.459)
16	18.1 (0.262)		21	24.9 (0.361)		30	42.6 (0.617)
17	19.4 (0.281)		22	26.4 (0.383)		35	56.4 (0.817)
18	20.6 (0.299)		23	28.1 (0.407)		40	73.9 (1.071)
19	22.0 (0.319)		24	29.9 (0.433)		45	95.9 (1.390)

- Temperature and Pressure Corrections:

The MilliGascounter is a volumetric gas meter and therefore measures gas volume in the actual operating state existing at the time of measurement. The gas volume is dependent on gas temperature, air pressure and water vapour partial pressure (for water vapour partial pressure refer to footnote “10“). These measurable variables are therefore needed to recalculate to STP conditions (see **eq. (51)**):

$$V_N = (V_i + V_D) \cdot \frac{P_a - P_V + P_L}{P_N} \cdot \frac{T_N}{T_a} \quad (51)$$

where V_N: measured volume at STP conditions dm³

V_i: indicated Volume dm³ by Rigamo software

V_D: deficit volume dm³

P_a: actual air pressure (If the exact air pressure is not known, the norm-pressure can in that case be used. Air pressure swings of 98 – 105 kPa create errors in the range of -3.3% to +3.7%.

P_V: water vapour partial pressure

P_L: Pressure of the liquid column above the measurement chamber = 1 mbar

P_N: STP-pressure = 1013.25 mbar

T_N: STP-temperature: 273.15 K

T_a: actual temperature in Kelvin

By substituting in **eq. 51** we got the measured gas volume at STP conditions see **eq (52)**. Two third of the produced gas is hydrogen – see **eq. (53)** – and one third of the produced gas is oxygen see **eq. (54)**

$$V_N = (0.8996 + 0.001315) \cdot \frac{1013.25 - 26.37 + 1}{1013.25} \cdot \frac{273.15}{295.15} = 0.813\ STP\ dm^3 \quad (52)$$

$$V_{H_2} = \frac{2}{3} \cdot V_N = \frac{2}{3} \cdot 0.813 = 0.542\ STP\ dm^3 \quad (53)$$

$$V_{O_2} = \frac{1}{3} \cdot V_N = \frac{1}{3} \cdot 0.813 = 0.271\ STP\ dm^3 \quad (54)$$

- **Comparison of the results:**

To compare the results, I defined indicators:

Theoretical electric efficiency see **eq. (55)**:

$$\eta_{teheo-ell} = \frac{E_{H_2}}{E} = \frac{n_{H_2}[mol] \cdot HHV_{H_2}[\frac{J}{mol}]}{E} = \frac{0.03 \cdot 286000]}{14005} = 60.9\% \quad (55)$$

Efficiency of volume measuring see **eq. (56)**:

$$\eta_{VM} = \frac{V_{measured}}{V_{total}} = \frac{0.813}{1.0023} = 81\% \quad (56)$$

Measured electric efficiency see **eq. (57)**:

$$\eta_{H_2} = \frac{\frac{V_{H_2}[dm^3\ measured\ H_2]}{V_M[\frac{mol}{dm^3\ STP\ gas}]} \cdot HHV_{H_2}[\frac{kJ}{mol}]}{E} = \frac{\frac{0.542}{22.414} \cdot 286[\frac{kJ}{mol}]}{14.005} = 49.4\% \quad (57)$$

3.5.2. Chronopotentiometry results

During the chronopotentiometry test, at a constant current of 800 mA, which corresponds to 35.7 mA cm^{-2}, the pure KOH solution without the C2 IL addition performed better. The C2 IL addition fastened the increment of the potential; however, the starting potential was lower in case of C2 addition (see **Figure 22B**). During the first chronopotentiometry test, the theoretically calculated gas volume based on the applied current, was more than the volume measuring device detected. Thus, indicated a failure in the reinforcement of the sealing, which means an additional parafilm layer was applied over the cell gasket. Afterward, when there was a parafilm layer under and over the cell gasket, the detected gas

volume was in balance with the theoretically calculated gas volume. The measurements with the C2 IL addition were done with the reinforced sealing (see **Figure 23A**). The difference between the addition of C2 IL, and the pure KOH solution in terms of the produced gas volume are minor (see **Figure 23B**).

Summary of chronopotentiometry measurements (see **Table 13, 14**):

- Using two layers of parafilm tape – one under and another one over the gasket – significantly increasing the measured gas volume.
- With C2mim addition 2.7 % more energy was used, comparing to without C2mim.
- With C2mim addition 3,5 % less gas was measured, comparing to without C2mim.
- With C2mim addition the H_2 production was 6.1 % less efficient, comparing to without C2mim.
- With C2mim addition the overall resistance was 2.7 % higher, comparing to without C2mim.

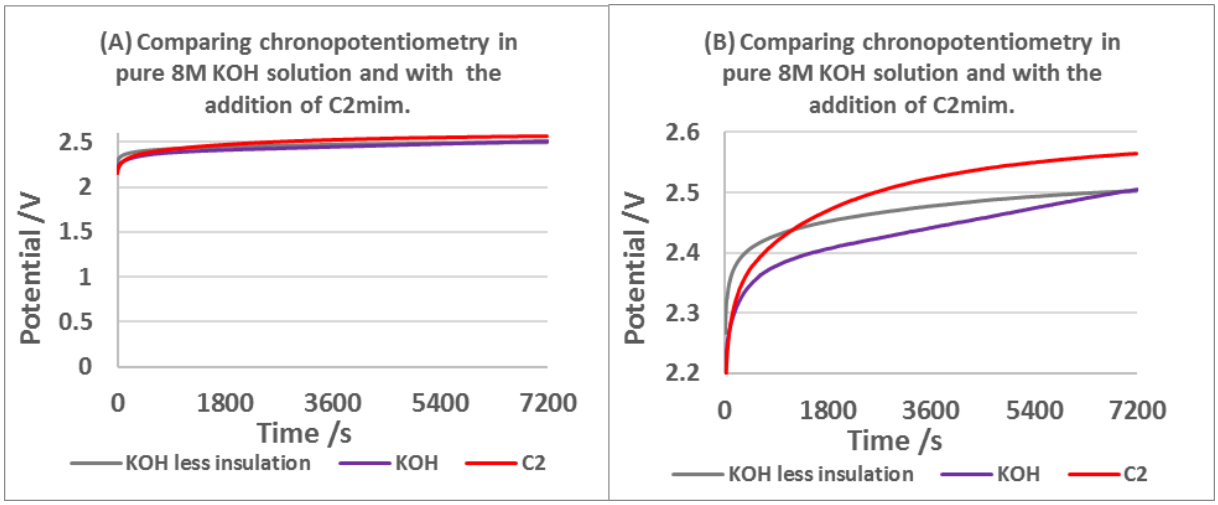

Figure 22. *Comparison of pure 8M KOH solution with and without the addition of C2 IL, during chronopotentiometry, whereas 800 mA were applied, which corresponds to 35.7 mA cm^{-2}. KOH less insulation data refers to use one additional paraffin layer for sealing the electrolysis cell, meanwhile KOH refers to use double paraffin layer for sealing. (A) with ranging potential of 0-2.6 V; (B) withy axis from 2.2 to 2.6 V.*

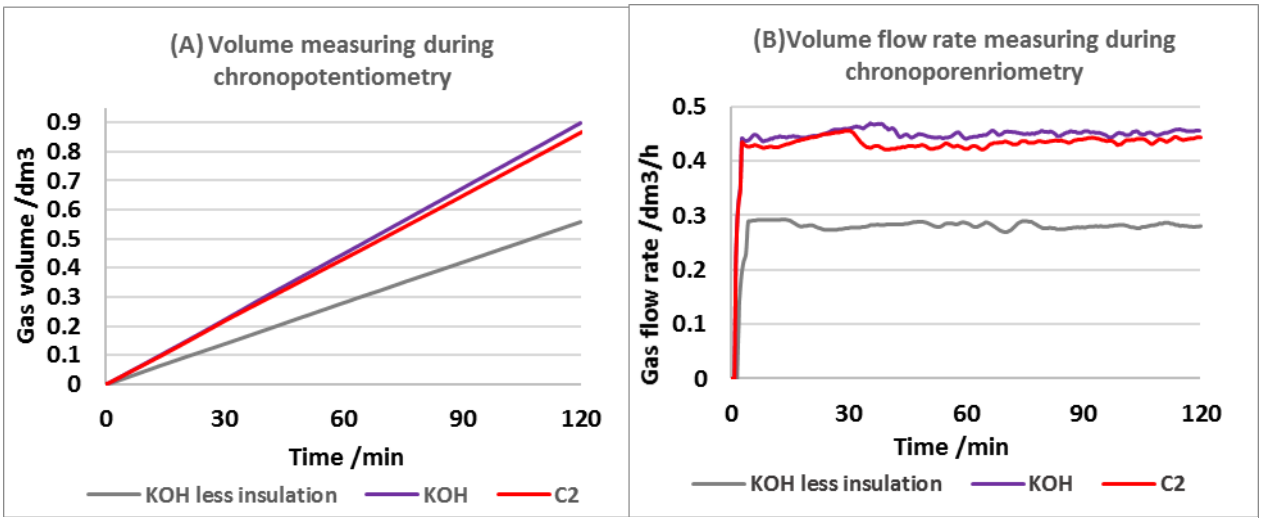

Figure 23. *(A) Comparison of volume measuring results using pure 8M KOH solution with and without the addition of C2 IL, during chronopotentiometry, whereas 800 mA were applied, which corresponds to 35.7 mA cm^{-2}. KOH less insulation data refers to use one additional paraffin layer for sealing the electrolysis cell, meanwhile KOH refers to use double paraffin layer for sealing. (B) Comparison of volume flow rate data using pure 8M KOH solution with and without the addition of C2 IL, during chronopotentiometry.*

Table 13. *Comparison of chronopotentiometry results with the specified indicators. E is the total energy used; Q is the total charge applied; V_{theo} is the theoretical produced gas volume; $\eta_{theo-ell}$ is the theoretical electric efficiency; η_{VM} is the efficiency of volume measuring; η_{H_2} is the measured electric efficiency.*

	KOH	C2mim	KOH less insulation
E[J]	14004.9	14380.2	14185.9
Q[C]	5753.0	5753.2	5749.9
$V_{theo}[STP\ dm^3]$	1.002	1.002	1.004
$V_N\ measured$ $[STP\ dm^3]$	0.813	0.784	0.506
$\eta_{theo-ell}$	0.609	0.593	0.602
η_{VM}	0.811	0.782	0.504
η_{H_2}	0.494	0.464	0.303

Table 14. *Comparison of the chronopotentiometry results by average current, average potential, and average resistance.*

	C2	KOH	KOH less insulation
AVG Current /mA	799.7	799.7	799.8
AVG Potential /mA	2.50	2.43	2.47
Resistance /Ω	3.13	3.04	3.08

3.5.3. Chronoamperometry results

During the chronoamperometry test at 2.3 V, the C2 IL additions significantly increased the current compared to pure 8M KOH solution. The C2 IL addition was increasing the starting current. The current was not decreasing faster than in the case of the pure 8M KOH solution, and the difference between currents was constant. The first test of pure 8M KOH with less insulation performed slightly better than with the reinforced insulation, but the final currents were similar (see **Figure 24**). The addition of C2 IL to the 8M KOH solution was significantly increased the volume flow rate as the volume flow rate shows a linear relationship with the current. In each case, the fast volume flow rate increment was followed by a short, but rapid decrease, and after that, the volume flow rate was decreasing slowly (see **Figure 25**). With the C2 IL addition, the volume flow rate was less stable, but still it was significantly higher, which in the end resulted in higher produced gas volume.

Summary of measurements (see **Table 15**,**16**):

- With C2mim addition 53.1 % more energy was used, comparing to without C2mim.
- With C2mim addition 37.4 % more gas was measured, comparing to without C2mim.
- With C2mim addition the H2 production was -10.2 % less efficient, comparing to without C2mim.
- With C2mim addition the overall resistance was 34.7 % smaller, comparing to without C2mim.

It is important to note, that with C2mim the current was significantly higher – which could be explained that the C2mim decreased the resistance of the system. It is a good sign to prove that C2mim can

significantly enhance water electrolysis. However, to compare the energy consumption, another device would be needed to measure how much energy was invested to maintain that constant potential.

It is not clear why C2mim performed better only during constant potential, meanwhile during constant current the results are similar.

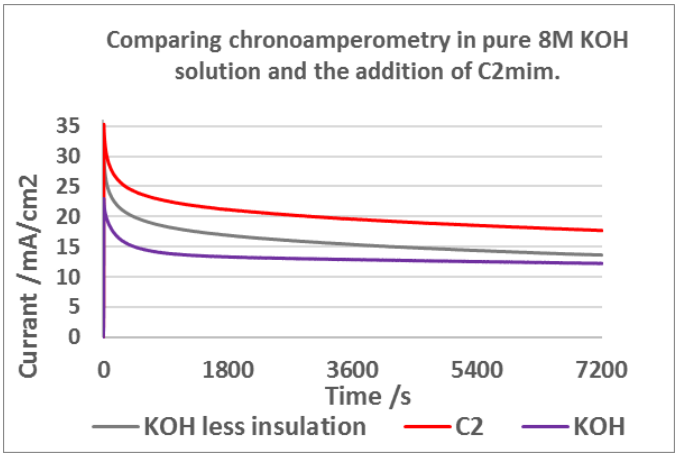

Figure 24. *Comparison of pure 8M KOH solution with and without the addition of C2 IL, during chronoamperometry, whereas 2.3 V were applied. KOH less insulation data refers to use one additional paraffin layer for sealing the electrolysis cell, meanwhile KOH refers to use of double paraffin layer for sealing.*

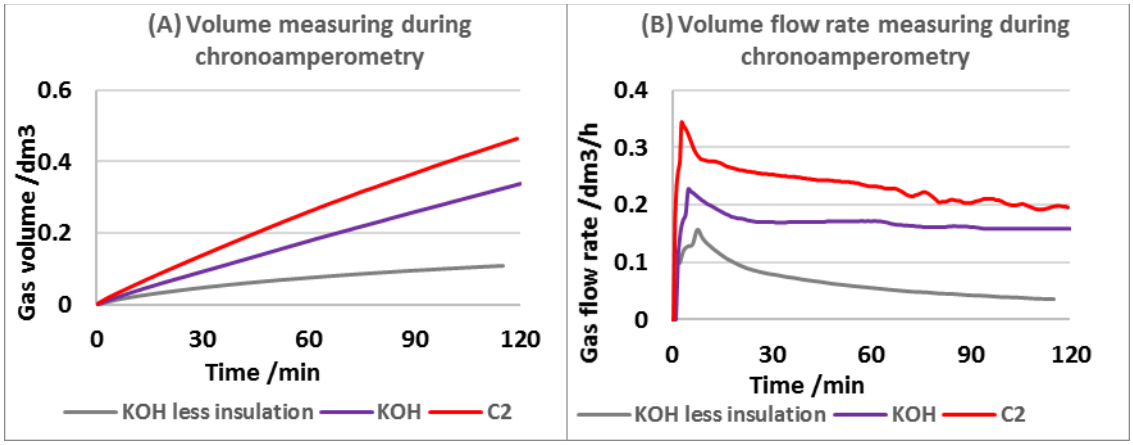

Figure 5. *(A) Comparison of the volume measurement results using pure 8M KOH solution with and without the addition of C2 IL, during chronoamperometry, whereas 2.3 V were applied. KOH less insulation data refers to use one additional paraffin layer for sealing the electrolysis cell, meanwhile KOH refers to use of additional paraffin layer for sealing. (B) Comparison of volume flow rate data using pure 8M KOH solution with and without the addition of C2 IL, during chronopotentiometry,*

Table 15. *Comparison of Chronoamperometry results with the specified indicators. E as the total energy used; Q as total charge applied; $Vtheo$ as Theoretical produced gas volume; $\eta theo-ell$ as theoretical electric efficiency; ηVM as Efficiency of volume measuring; $\eta H2$ as Measured electric efficiency.*

	KOH	C2mim	KOH less insulation
E[J]	4896.0	7493.8	5936.8
Q[C]	2128.8	3258.5	2581.3
$V_{theo}[STP\ dm^3]$	0.371	0.568	0.450
$V_N\ measured$ $[STP\ dm^3]$	0.305	0.419	0.099
$\eta_{theo-ell}$	0.644	0.644	0.644
η_{VM}	0.822	0.738	0.221
η_{H_2}	0.530	0.476	0.142

Table 16. *Comparison of Chronoamperometry results by average current average potential and average resistance.*

	C2	KOH	KOH less insulation
AVG Current /mA	435.7	284.5	358.6
AVG Potential /mA	2.27	2.27	2.30
Resistance / Ω	5.22	7.99	6.41

4. Conclusions

Minimizing the impact of global warming is a worldwide goal. In the Paris agreement, all nations agreed to put forward their best efforts through nationally determined contributions (NDCs) and to strengthen these efforts in the years ahead in order to keep global temperature rise this century well below 2 ºC above pre-industrial levels to avoid irreversible changes in the climate system [38]. In parallel with the Paris Agreement goals, the International Energy Agency (IEA) prepared a Sustainable Development Scenario (SDS) estimation about the global energy consumption in 2040. The main goal is to reduce the global CO_2 emission from 32.5 Gt CO_2/year (in 2017) to 17.5 Gt CO_2/year (in 2040) [7].

The main goals in the energy sector until 2040 by IEA are the followings [7]:

- Increase the global PV energy share in the global electricity production from 4.2% to 21.7%
- Increase the global Wind energy share in the global electricity production from 1.7% to 18%
- Increase the renewable energies (REs) share in the global heating sector from 10% to 25%
- Increase the REs share in the global transport sector from 3.5% to 19%
- Increase the REs share in the global electricity production from 19% to 66%

The installed PV and Wind plants are already causing grid instability, which will be even greater in the future according to SDS estimation. Power to gas (P2G) technologies are electricity storage systems,

which could produce hydrogen gas (H_2) and methane (CH_4). These P2G storage systems can stabilize the grid and, therefore, facilitate the penetration of PV and Wind plants, while offering valuable energy carriers such as H_2 and CH_4, which can then increase (REs) share in the global heating and transporting sector. One of the main components of these P2G plants is the water electrolyzer, which produces H_2 [8]. Nowadays 96% of H_2 is produced by carbon-based technologies, whereas the price ranges from 1-2 €/kg H_2. Currently, in the case of electrolyzers, this price is 3 €/kg H_2 [20] [15]. There are two commercialized water electrolysis technologies, one is the polymer membrane (PEM) electrolysis, the other one is alkaline electrolysis (AEL). Among these AEL is the more economically favourable because of the following [21]:

- This is the most mature and scaled up technology up to 2MW for one stack
- Longer lifetime
- Lower CAPEX

However, AEL still needs improvement in terms of efficiency, which can be increased by decreasing the ohmic overpotential or decreasing the activation overpotential. The activation overpotential can be decreased by selecting properly the electrode material, or by, what is the topic of this thesis, modifying the electrolyte by additives. In this thesis, four different methylimidazolium$^+$ based ILs were tested as electrolyte additives [28]. The catalytic effect of methylimidazolium$^+$-based and other ILs on HER were reported previously [32-34]. However, this catalytic effect of ILs is poorly described. The experiences with ILs and the potential explanations of their catalytic behaviour on HER and OER are the following:

- Investigation towards the alkyl chain length in Imidazolium$^+$ suggests that 4 carbon-atom long alkyl chain is the optimum length. A shorter chain would protect less the electrode surface, a longer chain would block too much of the electrochemically active surface area (ECAS) [35].
- Decreasing resistance related to mass and charge transfer, also decreases the overall impedance, and enhances HER kinetics [33, 34].
- Provides better adsorption on the electrode surface by helping cations to lose their solvation layer with the non-polar alkyl chains [36].
- Imidazolium$^+$ acts as a proton donor/acceptor thus providing a better proton donating effect and participating in the charge transfer reaction [31].
- Cations of IL form organised channels, perpendicular to the electrode surface [32].
- Prohibit Pt dissolution and suppress the formation of nonactive oxygenated species on the electrode surface [35].
- Imidazolium$^+$ is competing with the adsorbed H_2 molecules, thus facilitating H_2 desorption. Since imidazolium$^+$ acts as an H^+ donor and acceptor, it is participating in the charge transfer process and does not block active sites. These and other results indicate that the IL changes the electrolytic double layer (EDL) structure [36].
- The catalytic effect is related to the imidazolium$^+$ cation, which can be located near the anode in case of low potential, because at low potentials, a charge separated layer structure forms around the anode, whereas the proposition of the ions depends on the magnitude of the electrode surface [35].
- The shorter the alkyl chain, the slower the decomposition of the IL [37].

In this study, four different ILs were tested during HER and during OER as well. All of these four IL have chloride (Cl^-) anion, while the cations are: a) 3-Ethyl-1-methylimidazolium$^+$ chloride (C2); b) 3-Butyl-1-methylimidazolium$^+$ chloride (C4); c) 3-(2-Methoxyethyl)-1-methylimidazolium$^+$ chloride (C1OC2); and d) 3-(2-Ethoxyethyl)-1-methylimidazolium$^+$ chloride (C2OC2). With the rising of temperature, each ILs started to decompose. This degradation had a negative effect on the reaction kinetics, during HER. The optimal temperature range is between 25 ºC and 40 ºC, above this range, the current density started to decrease, except in the case of C2. However, even with the negative effect of the decomposition, the addition of ILs enhanced HER kinetics by:

- Increasing peak current density, decreasing onset potential, and shifting OCP to more positive values during cyclic voltammetry
- Increasing the exchange current density, decreasing E_{10} potential, and increasing j_{150} current density during LSV tests on 25 ºC and on 80 ºC as well.

The best results at 25 ºC were achieved with C1OC2 and C2 ILs, and at 80 ºC C2's results were outstanding which can be explained by the slower degradation of C2 than the degradation of C4. Thus, a higher concentration of imidazolium cations has a bigger catalytic effect on HER. It is not clear how the intermediate substances of the IL affect HER. On the other hand, the stability tests on 25 ºC brought contradictory results. Although HER in C2-containing electrolyte resulted in the highest starting current density, the current density was decreasing rapidly, and in the second half of the stability test, its value decayed below the value recorded in pure KOH results. Meanwhile, current density recorded using C1OC2- and C4-containing electrolytes started at lower values, but they were decreasing slower, and they were higher than values in pure KOH by the end of the two-hour stability test. Among the studied ILs, using C1OC2 resulted in the highest final current density. The difference between C2 and C1OC2 during the stability test is in line with the LSV results. Namely, using the two ILs resulted in similar current densities at -0.283 V (potential at which the stability tests was run) at 25 ºC, while C1OC2 outperformed C2 in the potential range of -0.10 V to -0.25 V. However, the better results obtained using C4 over ones obtained using C2 during stability test at 25 ºC were unexpected according to our LSV measurements. By contrast, C1OC2 and C2OC2 use as additives lead to the worst results during the stability test at 80 ºC. This means that even though they lead to a higher starting current density than the KOH, this current density was decreasing rapidly and felt below the pure KOH values in the first half of the test period. On the other hand, C2 and C4 gave significantly higher currents; moreover, a strange phenomenon appeared, when the current density is increasing during the stability test. This was also unexpected. It can be explained by experimental error, but this increase at 80 ºC was measured four times again during 80 ºC OER stability test. It is also possible that the later intermediates have a catalytic effect too. Otherwise, if the later intermediates do not affect the HER kinetics the current density should converge to the KOH curve. Therefore, further investigation of degradation is needed in form of longer stability tests at higher potentials. Also, the effect of intermediates of the ILs degradation is not clear as well. In summary of HER studies, ILs enhanced HER kinetics, in accordance with previous reports.

The effect of ILs on OER was not studied before. In our research, the ILs were starting to decompose with the elevation of temperature, as well as during HER measurements. The results of C2 IL are way too much better in terms of current density orders of magnitude higher compared to values with pure

KOH and other ILs, thus during those measurements an experimental error could have occurred. Other ILs significantly worsen OER kinetics which resulted in smaller peak current densities during CV test, and the smaller current densities above 2.03 V on the LSV records at 25 ºC. On the other hand - below 1.9 V - the OER reaction starts earlier with the addition of ILs. This can be explained by the assumption that IL ions would form a charge separated layer formation, with a changing anion-cation rich layer at the electrode surface, whereas the proposition of the ions depends on the magnitude of the electrode surface. Therefore, on lower potential the concentration of the active cations close to the positively charged anode is higher, hence their catalytic effect is higher as well. On the other hand, the lower current densities with the addition of ILs above 2.03 V is not explained. During LSV measurements C1OC2 IL appeared the most stable, and the curves are in accordance with the temperature rising. The performance of ILs in terms of current density at 25ºC during LSV are the following: C1OC2 < C2OC2 < C4, but the pure KOH outperformed each of them. C2 current density dropped drastically at 80 ºC. At 80 ºC each IL performed worse than the pure KOH solution. On the other hand, the OCP shifted to a more negative value, and the current density started to slowly increase much earlier –at 0.5 V - comparing to pure KOH solution where the onset point was 1.5 V. The Tafel plots show an enhancing effect of ILs on OER kinetics by:

- Increasing the exchange current density, decreasing E_{01} potential, and increasing j_{500} current density during LSV tests on 25 ºC

At 80 ºC only C1OC2 decreased E_{01} potential, other indicators were worse.

The stability tests show again a negative effect of the addition of ILs on OER kinetics. But current density increasing was again measured by adding C4 IL at 25 ºC. C2 results are outstanding, but can be related to a potential measuring failure. C1OC2 and C2OC2 produced almost zero current density, their trend is decreasing. At 80 ºC during the stability test, each ILs performed weakly comparing to pure KOH solution. Among ILs the order of performance is the following C2OC2<C4<C1OC2<(C2). The increasing current density was reported with each ILs. C1OC2, C4, and C1OC2 curves had parabolic increasing trend, meanwhile C2 curve had square root like increasing trend. The pure KOH curve was increasing as well, which was not expected, and might be related to an experimental error.

ILs have a different performance at different potential levels, also each of them starts to degrade by the increasing temperature. The degradation has a negative effect on the reaction kinetics. However, at 25ºC and at 80 ºC currents density increasing was observed several times, therefore further investigation on the degradation of ILs, and the effect of degradants on HER and on OER is adequate.

The future properties of an IL to be tailored in order to improve catalysis of OER are the followings:

- Anion in order to get closer to the anode on higher potential levels
- Having an amphipathic part which can help ions and the electrode surface to lose their solvation layer
- A molecule that can act as a hydroxide ion (OH^-) donor and acceptor; thus, the cation can take part in the electrochemical reaction and as a consequence the cation is not blocking ECAS. Similarly, the imidazolium$^+$ ion acts as a hydrogen ion (H^+) donor and acceptor.

In other words, an anion that has similar properties as the methyl-imidazolium^{+} ion + an alkyl chain group, since it is negatively charged it can be positioned much closer to the anode, than the methyl-imidazolium^{+} based cations.

Generated gas volume measurements were performed with a pure 8 M KOH solution and with the addition of C2 IL. The volume measuring was done during chronopotentiometry study, and during chronoamperometry study as well. During chronopotentiometry, the addition of C2 resulted in 3.5% less gas production; 6.1% less hydrogen production efficiency, and 2.7% higher average resistance. On the other hand, during chronoamperometry, the addition of C2 resulted in: 37.4% more gas production; 10.2% less hydrogen production efficiency, and 34.7 % smaller average resistance.

For further investigations, the volume measuring should be based on real-life industrial operation conditions, at around 200-400 mA cm^{-2} [39].

References

[1] S. Nian-Tzu, H. Sung-Fu, Q. Quan, Z. Nan, X. Yi-Jun and M. C. Hao, "Electrocatalysis for the oxygen evolution reaction: recent development and future perspectives," *Chemical Society Reviews,* vol. 46, pp. 337-365, 2017.

[2] M. Tahir, P. Lun, I. Faryal, Z. Xiangwen, W. Li, Z. Ji-Jun and L. W. Zhon, "Electrocatalytic oxygen evolution reaction for energy conversion and storage: A comprehensive review," *Nano Energy,* vol. 37, pp. 136-157, 2017.

[3] "2019 United Nations Framework Convention on Climate Change," United Nations Framework Convention on Climate, [Online]. Available: https://unfccc.int/sites/default/files/english_paris_agreement.pdf. [Accessed 30 09 2019].

[4] T. Lenton M., H. Held, E. Kriegler, J. W. Hall, W. Lucht, S. Rahmstorf and H. J. Schellnhuber, "Tipping elements in the Earth's climate system," *PNAS,* vol. 105, pp. 1786-1793, 2008.

[5] B. Goswami, N. Boers and P. Ditlevesen, "meetingorganizer.copernicus.org: Tipping Points in the Earth System: An introduction to the TiPES project," 2019. [Online]. Available: https://meetingorganizer.copernicus.org/EGU2019/EGU2019-18084.pdf. [Accessed 30 9 2019].

[6] M. Bindi, S. Brown, O. Hoegh-Guldberg and I. Camilloni, "ipcc.ch; Impacts of 1.5ºC of Global Warming on Natural and Human Systems," [Online]. Available: https://www.ipcc.ch/site/assets/uploads/sites/2/2019/02/SR15_Chapter3_Low_Res.pdf. [Accessed 30 09 2019].

[7] "https://www.iea.org/weo2018/scenarios/," International Energy Agency, 2019. [Online]. Available: iea.org/weo2018. [Accessed 25 9 2019].

[8] D. Parra and K. M. Patel, "Techno-economic implications of the electrolyser," *International Journal of Hydrogen Energy,* vol. 41, pp. 3748-3761, 2016.

[9] O. Takaya, T. Mizumoto and K. Yuya, “Analysis of Trends and Emerging Technologies in Water Electrolysis Research Based on a Computational Method: A Comparison with Fuel Cell Research,” *Sustainability,* vol. 10, pp. 478/1-478/24, 2018.

[10] S. Weidner, M. Faltenbacher, I. Francois, D. Thomas, J. Skulason and C. Maggi, “Feasibility study of large scale hydrogen power-togas applications and cost of the systems evolving with scaling up in Germany, Belgium and Iceland,” *International Journal of Hydrogen Energy,* vol. 43, pp. 15625-15638, 2018.

[11] C. Acar and I. Dincer, “Review and evaluation of hydrogen production options for better environment,” *Journal of Cleaner Production,* vol. 218, pp. 835-849, 2019.

[12] S. K. Shiva and V. Himabindu, “Hydrogen production by PEM water electrolysis – A review,” *Materials Science for Energy Technologies,* vol. 2, pp. 442-454, 2019.

[13] R. Md Mamoon, K. M. Al Mesfer, H. Naseem and M. Danish, “Hydrogen Production by Water Electrolysis: A Review of Alkaline Water Electrolysis, PEM WaterElectrolysis and High Temperature Water Electrolysis,” *International Journal of Engineering and Advanced Technology,* vol. 4, pp. 80-93, 2015.

[14] “https://www.iea.org/topics/hydrogen/whyhydrogen/,” International Energy Agency, [Online]. Available: https://www.iea.org/topics/hydrogen/whyhydrogen/.

[15] “The Future of HydrogenReport prepared by the IEAfor the G20, JapanSeizing today’s opportunities,” International Energy Agency, 2019.

[16] “https://www.energy.gov/eere/fuelcells/hydrogen-production-processes,” U.S Department of Energy. [Online]. [Accessed 26 10 2019].

[17] M. Ahmed and I. Dincer, “A review on photoelectrochemical hydrogen production systems: Challenges and future directions,” *International Journal of Hydrogen Energy,* vol. 44, pp. 2474-2507, 2019.

[18] Y. Jingang, M. Kraussler, F. Benedikt and H. Hofbauer, “Techno-economic assessment of hydrogen production based on dual fluidized bed biomass steam gasification, biogas steam reforming, and alkaline water electrolysis processes,” *Energy Conversion and Management,* vol. 145, pp. 278-292, 2017.

[19] S. Saeidi, F. Fazlollahi, S. Najari, I. Davood, J. K. Jaromír and L. L. Baxter, “Hydrogen production: Perspectives, separation with special emphasis on kinetics of WGS reaction: A state-of-the-art review,” *Journal of Industrial and Engineering Chemistry,* vol. 49, pp. 1-25, 2017.

[20] J. Proost, “State-of-the art CAPEX data for water electrolysers, and their impact on renewable hydrogen price settings,” *International Journal of Hydrogen Energy,* vol. 44, pp. 4406-4413, 2019.

[21] J. Koponen, A. Kosonen and J. Ahola, “Review of water electrolysis technologies and design of renewable hydrogen production systems Progress of Master’s Thesis,” NEO-CARBON ENERGY, Lappeenranta Univesity of Technology, 2016.

[22] I. Vincent and D. Bessarabov, “Low cost hydrogen production by anion exchange membrane electrolysis: A review,” *Renewable and Sustainable Energy Reviews,* vol. 81, pp. 1690-1704, 2018.

[23] M. S. Foteini, J. M. Garcia, C. Weststrare, H. O. Fredriksson and J. Niemantsverdriet, “Electrocatalysts for the generation of hydrogen, oxygen and synthesis gas,” *Progress in Energy and Combustion Science,* vol. 58, pp. 1-35, 2017.

[24] W. Vielstich, A. Lamm, H. A. Gasteiger and A. Lasia, “Hydrogen Evolution Reaction,” *Handbook of Fuel Cells – Fundamentals, Technology and Applications,* pp. 416-440, 2003.

[25] C. M. A. Brett and A. M. O. Brett, ELECTROCHEMISTRY, Oxford New York Tokyo: OXFORD UNIVERSITY PRESS, 1994.

[26] S. Nian-Tzu, H. Sung-Fu, Q. Quan, Z. Nan, X. Yi-Jun and M. C. Hao, “Electrocatalysis for the oxygen evolution reaction: recent development and future perspectives,” *Chemical Society Reviews,* vol. 46, pp. 337-365, 2017.

[27] R. L. Doyle and M. E. Lyons, “Chapter 2 The Oxygen Evolution Reaction: Mechanistic Concepts and Catalyst Design,” Springer International Publishing Switzerland 2016, 2016, pp. 41-104.

[28] D. Martín, C. Ocampo-Martínezc and R. Sánchez-Peña, “Advances in alkaline water electrolyzers: A review,” *Journal of Energy Storage,* vol. 23, pp. 392-403, 2019.

[29] H. Liu and H. Yu, “Ionic liquids for electrochemical energy storage devices applications,” *Journal of Materials Science & Technology,* vol. 35, pp. 674-686, 2019.

[30] R. F. Souza, J. C. Padilha, R. S. G. Gonçalves, M. O. Souza. and J. Rault-Berthelot, “Electrochemical hydrogen production from water electrolysis using ionic liquid as electrolytes: Towards the best device,” *Journal of Power Sources,* vol. 164, pp. 732-738, 2007.

[31] R. F. Souza, L. Gabriel, J. C. Padilha, M. M. Emilse and M. O. Souza, “Molybdenum electrodes for hydrogen production by water electrolysis using ionic liquid electrolytes,” *Electrochemistry Communications,* vol. 10, pp. 1673-1675, 2008.

[32] F. Fiegenbaum, M. O. Souza, M. R. Becker, M. Emilse M.A. and R. F. Souza, “Electrocatalytic activities of cathode electrodes for water electrolysis using tetra-alkyl-ammonium-sulfonic acid ionic liquid as electrolyte,” *Journal of Power Sources,* vol. 280, pp. 12-17, 2015.

[33] L. Amaral, D.S.P. Cardoso, B. Šljukić, D.M.F. Santos and C.A.C. Sequeira, “Room Temperature Ionic Liquids as Electrolyte Additives for the HER in Alkaline Media,” *Journal of The Electrochemical Society,* vol. 164, F427-F432, 2017.

[34] L. Amaral, J. Minkiewicz, B. Šljukić, D.M.F. Santos, C.A.C. Sequeira, M. Vranes and S. Gadzuric, “Toward Tailoring of Electrolyte Additives for Efficient Alkaline Water Electrolysis: Salicylate-Based Ionic Liquids,” *ACS Applied Energy Materials,* vol. 1 (9), pp. 4731-4742, 2018.

[35] G.-R. Zhang, T. Wolker, D. J. Sandbeck, M. Munoz, K. J. J. Mayrhofer, S. Cherevko and B. J. Etzold, “Tuning the Electrocatalytic Performance of Ionic Liquid Modified Pt Catalysts for Oxygen

Reduction Reaction via Cationic Chain Engineering," *ACS Catalysis,* vol. 8 (9), pp. 8244-8254, 2018.

[36] L. Zanchet, L. G. Trindade, D. W. Lima, W. Bariviera, F. Trombetta, M. O. d. Souza and E. M. A. Martini, "Cation influence of new imidazolium-based ionic liquids on hydrogen production from water electrolysis," *Ionics,* vol. 25, p. 1167–1176, 2019.

[37] J. Gao, L. Chen, Y. He, Z. Yan and X. Zheng, "Degradation of imidazolium-based ionic liquids in aqueous solution using plasma electrolysis," *Journal of Hazardous Materials,* vol. 263, pp. 261-270, 2014.

[38] U. N. C. change, "https://unfccc.int," [Online]. Available: https://unfccc.int/process-and-meetings/the-paris-agreement/the-paris-agreement.

[39] Y. Guo, G. Li, J. Zhou and Y. Liu, "Comparison between hydrogen production by alkaline water," in *IOP Conference Series: Earth and Environmental Science 371*, Beijing, 2019.

[41] R. Warren, O. Andrews and B. Sally, "Risks associated with global warming". *Tyndall℃Centre for Climate Change Research.*

[42] C. S. a. s. chemistry, "http://www.chemspider.com," 2019. [Online]. Available: http://www.chemspider.com. [Accessed 1 4 2019].

[43] C. Samori, G. Scuitto and L. Pazzolesi, "Effects of Imidazolium Ionic Liquids on Growth, Photosynthetic Efficiency, and Cellular Components of the Diatoms Skeletonema marinoi and Phaeodactylum tricornutum," *Chemical Research in Toxicology,* vol. 24, pp. 392-401, 2011.

[44] M. I. El-Snafie, H. Yukio and K. Shinji, "Hydrogen Production Technologies Overview," *Journal of Power and Energy Engineering,* vol. 7, pp. 107-154, 2019.

[45] T. O'Riordan and T. Lenton, "Addressing Tipping Points for a Precarious Future: Tipping Elements from a Global Perspective," *British Academy Scholarship Online,* 2013.